Sensitivity Analysis of Wind Characteristics and Turbine Properties on Wind Turbine Loads

Amy N. Robertson[1], Kelsey Shaler[1], Latha Sethuraman[1], Jason Jonkman[1]

[1]National Renewable Energy Laboratory, 15013 Denver West Parkway, Golden, CO 80401, USA

5   *Correspondence to*: Amy N. Robertson (amy.robertson@nrel.gov)

Abstract. Wind turbine design relies on the ability to accurately predict turbine ultimate and fatigue loads. The loads analysis process requires precise knowledge of the expected wind-inflow conditions as well as turbine structural and aerodynamic properties. However, uncertainty in most parameters is inevitable. It is therefore important to understand the impact such uncertainties have on the resulting loads. The goal of this work is to assess which input parameters have the greatest influence
10   on turbine power, fatigue loads, and ultimate loads during normal turbine operation. An Elementary Effects (EE) sensitivity analysis is performed to identify the most sensitive parameters. Separate case studies are performed on 1) wind-inflow conditions and 2) turbine structural and aerodynamic properties, both using the National Renewable Energy Laboratory (NREL) 5-MW baseline wind turbine. The Veers model was used to generate synthetic IEC Kaimal turbulence spectrum inflow. The focus is on individual parameter sensitivity, though interactions between parameters are considered.
15
The results of this work show that for wind-inflow conditions, turbulence in the primary wind direction and shear are the most sensitivity parameters for turbine loads, which is expected. Secondary parameters of importance are identified as veer, u-direction integral length, and components of the IEC coherence model, as well as the exponent. For the turbine properties, the most sensitive parameters are yaw misalignment and outboard lift coefficient distribution. This information can be used to
20   help establish error bars around the predictions of engineering models during validation efforts, and provide insight to probabilistic design methods and site-suitability analyses.

1 Introduction

Wind turbines are designed using the IEC 61400-1 standard, which prescribes a set of simulations to ascertain the ultimate and fatigue loads that the turbine could encounter under a variety of environmental and operational conditions. The standard applies
25   safety margins to account for the uncertainty in the process, which comes from the procedure used to calculate the loads (involving only a small fraction of the entire lifetime), but also from uncertainty in the properties of the system, variations in the conditions the turbine will encounter from the prescribed values, and modeling uncertainty. As manufacturers move to develop more advanced wind technology, better optimized designs, and reduce the cost of wind turbines, it is important to better understand how uncertainties impact modeling predictions and reduce the uncertainties where possible. Knowledge of
30   where the uncertainties stem from can lead to a better understanding of the cost impacts and design needs of different sites and different turbines.

This paper provides a better understanding of the uncertainty in the ultimate and extreme structural loads and power in a wind turbine. This is done by parameterizing the uncertainty sources; prescribing a procedure to estimate the load sensitivity to each
35   parameter; and identifying which parameters have the largest sensitivities for a conventional utility-scale wind turbine under normal operation. An Elementary Effects methodology was employed for estimating the sensitivity of the parameters. This approach was chosen as it provides a reasonable estimate of sensitivity, but with significantly less computational requirements compared to calculating the Sobol sensitivity, and without increasing the uncertainty in the result through the use of a reduced-order model. Some modifications were needed to the standard Elementary Effects approach to properly compare loads across
40   different wind speed bins.

This work is a first step in understanding potential design process modifications to move towards a more probabilistic approach or to inform site-suitability analyses. The results of this work can be used to 1) rank the sensitivities of different parameters, 2) help establish error bars around the predictions of engineering models during validation efforts, and 3) provide insight to probabilistic design methods.

5 ## 2 Analysis Approach

2.1 Overview

To identify the most influential sources of uncertainty in the calculation of the structural loads for utility-scale wind turbines, a sensitivity analysis methodology based on Elementary Effects (EE) is employed. The focus is on the sensitivity of the input parameters of wind turbine simulations (used to calculate the loads), not on the modeling software itself, which creates
10 uncertainty based on whether the approach used accurately represents the physics of the wind loading and structural response. The procedure followed is summarized in the following sub-sections. The caveats of the sensitivity analysis approach employed are given as follows:

- Only the NREL 5-MW reference turbine is used to assess sensitivity (the resulting identification of most-sensitive parameters may depend on the turbine).
15 - Only normal operation under turbulence is considered (gusts, start-ups, shut-downs, and parked/idling events are not considered).
- Min/max values of the input parameter uncertainty ranges are examined in the analysis (no joint probability density function is considered).
- With the exception of wind speed, each parameter is examined independently across the full range of variation, and
20 is not conditioned based on other parameters.

2.2 Wind turbine model and tools

The sensitivity due to each input parameter on turbine load response is assessed through the use of a simulation model. The NREL 5-MW reference turbine (Jonkman et al., 2009) was used in this study as a representative turbine. This is a variable-speed, 3-bladed, upwind, horizontal-axis turbine with a hub height of 90 m and a rotor diameter of 126 m. Though not covered
25 in this work, it would also be useful to examine in future work how the sensitivity of the parameters on turbine loads is affected by the size and type of the considered wind turbine.

The effect of input parameters on load sensitivity could be influenced by the wind speed and associated wind turbine controller response. Therefore, the EE analysis was performed at three different wind speeds corresponding to mean hub height wind
30 speeds of 8, 12, and 18 m/s, representing below-, near-, and above-rated wind speeds, respectively. Turbulent wind conditions were generated at each wind speed using TurbSim (Jonkman, 2009), employing an IEC Kaimal turbulence spectrum with exponential spatial coherence. Multiple turbulence seeds were used for each input parameter variation to ensure the variation from input parameter changes is distinguishable from the variation of the selected turbulence seed. The number of seeds was determined through a convergence study for each of the parameter sets. A 25 x 25 point square grid of three-component wind
35 vector points that encompasses the turbine rotor plane was used.

OpenFAST, a state-of-the-art engineering-level aero-servo-elastic modeling approach, was used to simulate the NREL 5-MW wind turbine using the developed wind files, allowing for aeroelastic response and turbine operation analysis. A simulation time of 10 minutes was used after an initial 30-second transient period per turbulence seed. Drag on the tower was not
40 considered because it is negligible for an operational turbine. AeroDyn, the aerodynamic module of OpenFAST, determines the impact of the turbine wake using induction factors that are computed using blade-element momentum (BEM) theory with advanced corrections. Steady and unsteady aerodynamic response were considered. Steady aerodynamic modeling uses static lift and drag curves in the momentum balance to calculate the local induction. Unsteady airfoil aerodynamic modeling accounts for dynamic stall, flow separation, and flow reattachment to calculate the local aerodynamic applied loads. ElastoDyn, a

combined multibody and modal structural approach that includes geometric nonlinearities, was used to represent the flexibility of the blades, drivetrain, and tower and compute structural loading, which was used to compute ultimate and fatigue loads. The baseline controller of the NREL 5-MW turbine was enabled using ServoDyn. OpenFAST results were used to assess the change in response quantities of interest (QoIs) to changes in the physical input parameters.

5 **2.3 Case Studies**

Input parameters were identified that could significantly influence the loading of a utility-scale wind turbine. These parameters were organized into two main categories (or case studies): the ambient wind-inflow conditions that will generate the aerodynamic loading on the wind turbine and the aeroelastic properties of the structure that will determine how the wind turbine will react to that loading (see Figure 1). Within these two categories, a vast number of uncertainty sources can be 10 identified, and Abdallah (2015) provides an exhaustive list of the properties. For this study, the authors selected those parameters believed to have the largest effect for normal operation for a conventional utility-scale wind turbine, which are categorized into the labels shown in Figure 1.

To understand the sensitivity of a given parameter, a range over which that parameter may vary needed to be defined. For the 15 wind conditions, a literature search was done to identify the reported range for each of the parameters across different potential wind-farm locations within the three wind speed bins. For the aeroelastic properties, the parameters are varied based on an assessed level of potential uncertainty associated with each parameter.
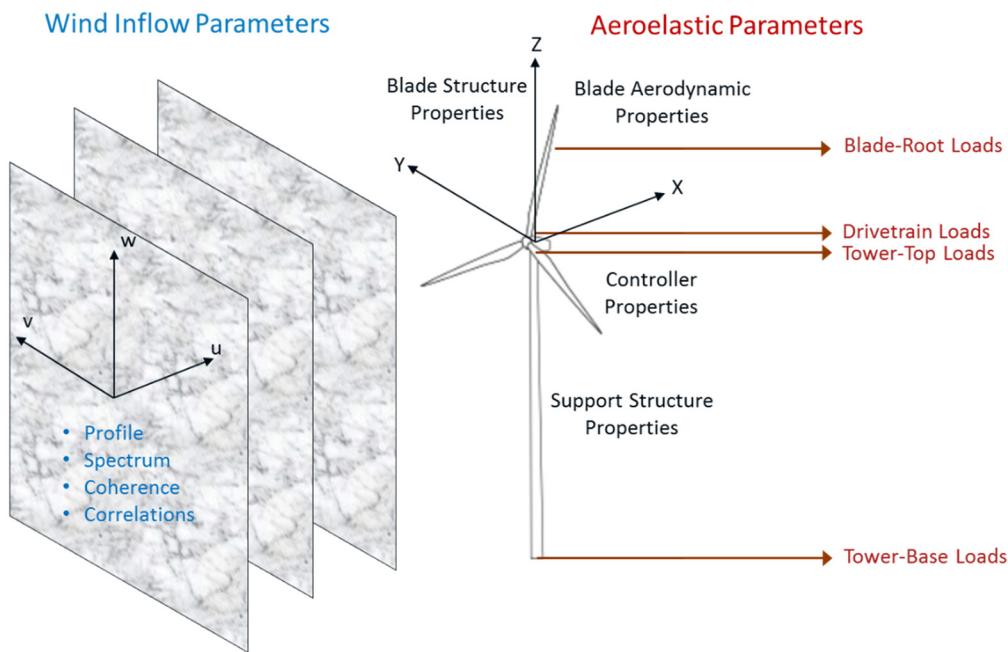
Figure 1: Overview of the parametric uncertainty in a wind turbine loads analysis. Includes wind-inflow conditions (subset shown 20 in blue), turbine aeroelastic properties (subset shown in black), and the associated load QoI (subset shown in red).

2.4 Quantities of Interest

To capture the variability of turbine response that results from parameter variation, several QoIs were identified. These QoIs are summarized in Table 1 and include the blade, drivetrain, and tower loads; blade-tip displacement; and turbine power. Ultimate and fatigue loads were considered for all load QoIs, whereas only ultimate values were considered for blade-tip 25 displacements. The ultimate loads were estimated using the average of the global absolute maximums across all turbulence

seeds for a given set of parameter values. The fatigue loads were estimated using damage-equivalent loads (DEL) of the QoI response across all seeds for a given set of parameter values. For the bending moments, the ultimate loads were calculated as the largest vector sum of the first two components listed, rather than considering each individually. The QoI sensitivity of each input parameter is examined using the procedure summarized in the next section.

Table 1. Quantities of interest examined in the sensitivity analyses.

Quantity of Interest	Component		
Blade-root moments	Out-of-plane bending	In-plane bending	Pitching moment
Low-speed shaft moments at main bearing	0-degree bending	90-degree bending	Shaft torque
Tower-top moment	Fore/aft bending	Side/side bending	Yaw moment
Tower-base moment	Fore/aft bending	Side/side bending	
Blade-tip displacement	Out-of-plane (Ultimate only)		
Electrical power			

3 Sensitivity Analysis Procedure

3.1 Sensitivity Analysis Approaches

There are many different approaches to assess the sensitivity of the QoI for a given input parameter. The best choice depends on the number of considered input parameters, simulation computation time, and availability of parameter distributions.

10   Sensitivity is commonly assessed through the Sobol sensitivity (Saltelli et al., 2008), which decomposes the variance of the response into fractions that can be attributed to different input parameters and parameter interactions. The drawback of this method is the large computational expense, which requires a Monte Carlo analysis to calculate the sensitivity. To decrease the computational expense, one approach is to use a meta-model, which is a lower-order surrogate model trained on a subset of simulations to capture the trends of the full-order, more computationally expensive model. This approach has been used in the

15   wind energy field (Nelson et al., 2003; Rinker, 2016; Sutherland, 2002; Ziegler et al., 2016), but was deemed unsuitable for this work given the wind turbine model complexity and associated QoIs. Specifically, it may be difficult for a meta-model to capture the system nonlinearities and interaction of the controller, especially the ultimate loads, limiting meta-model accuracy. Another approach to reduce computational expense is to use a design of experiments approach to identify the fewest simulations needed to capture the variance of the parameters and associated interactions, *e.g.*, Latin hypercube sampling

20   (Matthaus et al., 2017; Saranyasoontorn, 2006; Saranyasoontorn et al., 2008) and fractional factorial analysis (Downey, 2006). These methods were considered for this application, but such approaches are still too computationally expensive given the large number of considered input parameters. Instead, a screening approach was determined to be the best approach. A screening method provides a sensitivity measure that is not a direct estimate of the variance, but rather supplies a ranking of those parameters with the most influence. One of the most commonly used screening approaches is called Elementary Effect

25   (EE) analysis (Compolongo et al., 2007; Campolongo et al., 2011; Francos et al., 2003; Gan, 2014; Huang et al., 2012; Jansen, 1999; Martin et al., 2016; Saint-Geours et al., 2010; Soheir et al., 2015). Once the EE analysis identifies the input parameters that are most influential to the QoIs, a more targeted analysis can be performed using one of the other sensitivity analyses discussed above.

3.2 Overview of Elementary Effects

30   EE at its core is a simple methodology for screening parameters. It is based on the one-at-a-time approach in which each input parameter of interest is varied individually while holding all other parameters fixed. A derivative is then calculated based on the level of change in the QoI to the change in the input parameter using first-order finite differencing. Approaches such as these are called local sensitivity approaches because they calculate the influence of a single parameter without considering interaction with other parameters. However, the EE method extends this process by examining the change in response for a

given input parameter at different locations (points) in the input parameter hyperspace. In other words, only one parameter is varied at a time, but this variation is performed multiple times using different values for the other input parameters, as shown in Figure 2. The derivatives calculated from the different points are considered to assess an overall level of sensitivity. Thus, the EE method considers the interactions between different parameters and is therefore considered a global sensitivity analysis method.
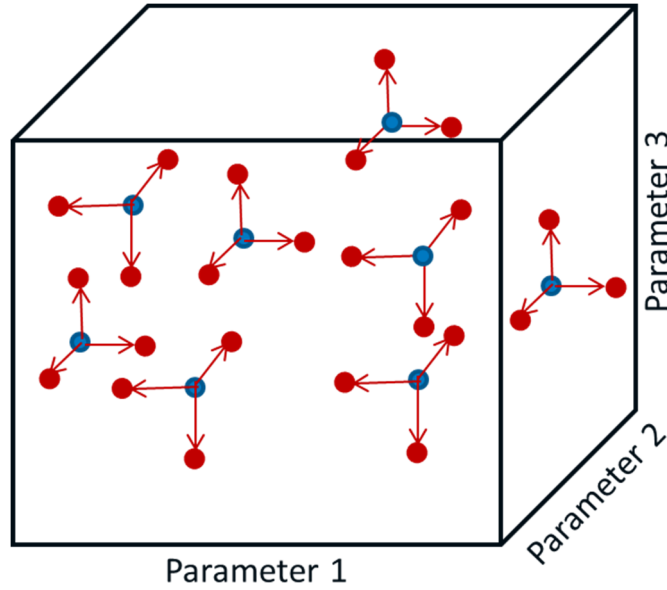
Figure 2: Radial EE approach representation for 3 input parameters. Blue circles indicate starting points in the parameter hyperspace. Red points indicate variation of one parameter at a time. Each variation is performed for 10% of the range over which the parameter may vary, either in the positive or negative direction.

Each wind turbine QoI, **Y**, is represented as a function of different characteristics of the wind or model property input parameters, **U**, as follows:

$$\mathbf{Y} = f(u_1, \ldots, u_i, \ldots, u_I) \tag{1}$$

where I is the total number of input parameters. In the general EE approach, all input parameters are normalized between 0 (minimum value) and 1 (maximum value). For a given sampling of **U**, the EE value of the input parameter, i, is found by varying only that parameter by a normalized amount, Δ:

$$EE_i = \frac{f(\mathbf{U}+x_k)-f(\mathbf{U})}{\Delta} \tag{2}$$

where

$$x_k = \begin{cases} 0 & \text{for } k \neq i \\ \Delta & \text{for } k = i \end{cases} \tag{3}$$

Because of the normalization of **U**, the elementary effect value (EE_i) can be thought of as the local partial derivative of the **Y** with respect to an input (u_i), scaled by the range of that input. Thus, the EE value has the same unit as the output QoI. The EE value is calculated for R starting points in the input parameter hyperspace, creating a set of R different calculations of EE value for each input parameter.

The basic approach for performing an EE analysis has been modified over the years to ensure that the input hyperspace is being adequately sampled and to eliminate issues that might confound the sensitivity assessment. In this work, the following modifications to the standard approach were made:

1. A radial approach, where the EE values were calculated by varying each parameter one at a time from a starting point (see Figure 2), was used rather than the traditional trajectories for varying all of the parameters, which has been shown to improve the efficiency of the method (Campolongo et al., 2011).
2. Sobol numbers were used to determine the initial points at which the derivatives will be calculated (blue circles in Figure 2), which ensures a wide sampling of the input hyperspace (Campolongo et al., 2011; Robertson et al., 2018).
3. A set delta value equal to 10% of the input parameter range ($\Delta_{ib} = \pm 0.1 u_{ib,\text{range}}$) was used to ensure the calculation of the finite difference occurred over an appropriate range to better meet the assumption of linearity.
4. A modified EE formula—different for ultimate and fatigue loads—was used to examine the sensitivity of the parameters across multiple wind speed bins. EE modifications are detailed in Sections 3.3.1 and 3.3.2.

3.3 Elementary Effects Formulas

This section provides the detailed formulas used to calculate the EE values for the ultimate and fatigue loads.

3.3.1 Ultimate Loads

When considering the ultimate loads, only the single highest ultimate load is of concern, regardless of the wind speed bin. Therefore, the standard EE formula is modified so that the sensitivity of the parameters can be examined consistently across different wind speed bins. This is accomplished by keeping $\mathbf{U}$ and Δ dimensional (i.e., not making $\mathbf{U}$ dimensionless between 0 and 1), multiplying the derivative, approximated with a finite difference, by the total range of the input for a given wind speed bin, and adding the nominal value of the QoI associated with IEC turbine class I and category B (IEC Class IB) for the given wind speed bin. The EE of input parameter U_{ib}^r for a certain QoI, $\mathbf{Y}$, at starting point r in wind speed bin b is then given by:

$$EE_{ib}^r = \left| \frac{Y(\mathbf{U}^r + x_k) - Y(\mathbf{U}^r)}{\Delta_{ib}} u_{ib,\text{range}} \right| + \bar{Y}_b \qquad (4)$$

where $\bar{Y}_b$ represents the IEC Class IB nominal value for the given wind speed bin; and the ultimate load, $Y(\mathbf{U})$, is defined as the mean of the absolute maximum of the temporal response load in bin b across S seeds for a certain input parameter i and starting point r:

$$Y(\mathbf{U}^r) = \frac{1}{S} \sum_{s=1}^{S} MAX(|Y(\mathbf{U}^r)|) \qquad (5)$$

3.3.2 Fatigue Loads

To compute the fatigue loads, the same basic formulation is used as for the ultimate loads, but the DEL of the temporal response is considered in place of the mean of the absolute maximums:

$$EE_{ib}^r = P(v_b) \left| \frac{DEL(\mathbf{U}^r + x_k) - DEL(\mathbf{U}^r)}{\Delta_{ib}} u_{ib,\text{range}} \right| \qquad (6)$$

where $DEL(\mathbf{U}^r)$ is the aggregate of the short-term DEL of a given QoI across all seeds computed using the NREL post-processing tool, MLife (Hayman et al., 2012). DELs are computed without the Goodman correction and with load ranges about

a zero fixed mean. The fatigue EE value is scaled by $P(v_b)$, which is the Rayleigh probability at the wind speed v_b (assuming IEC Class IB turbulence) associated with bin b to compare the fatigue loads consistently across wind speed bins.

3.4 Identification of Most Sensitive Inputs

The EE value is a surrogate for a sensitivity level. Therefore, a higher EE value for a given input parameter indicates more
5   sensitivity. Here, the most sensitive parameters are identified by defining a threshold over which an individual EE value would be considered significant, indicating the sensitivity of the associated parameter. This approach differs from the classical method of determining parameter sensitivity, as discussed in Appendix A. The threshold is set individually for each QoI. For the wind parameter study, the threshold is defined as $\overline{EE^r} + 2\sigma$, where $\overline{EE^r}$ is the mean of all EE values across all starting points R, inputs I, and wind speed bins B for each QoI, and σ is the standard deviation of these EE values. For the turbine parameter
10   study, the results are stratified based on wind speed bin. Therefore, the threshold for this study is modified to $\overline{EE^r} + 1.7\sigma$. Additionally, the ultimate load thresholds for the turbine parameter study are computed using only near- and above-rated results because of the separation of EE values between the below-, near-, and above-rated wind speed bins. For both studies, fatigue load EE values are not clearly separated by wind speed; therefore, all wind speeds are used to compute the fatigue load parameter thresholds.

15 **4 Results**

Two separate case studies were performed to assess the sensitivity of input parameters on the resulting ultimate and fatigue loads of the NREL 5-MW wind turbine. The categories of input parameters analyzed were the wind-inflow conditions and the aeroelastic turbine properties. In both of the case studies, loads were analyzed for three wind speed bins, using mean wind speed bins of 8, 12, and 18 m/s, representing below-, near-, and above-rated wind speed bins, respectively. Turbulent wind
20   conditions were generated using an IEC Kaimal turbulence spectra with exponential spatial coherence functions. For the turbine parameter study, turbulence was based on IEC Class IB turbulence. Correlations and joint distributions of the parameters were not considered since developing this relationship for so many parameters would be difficult or impossible. In addition, the correlation could be very different for different wind sites. The impact of not considering the correlation was limited by choosing parameters that were fairly independent of one another, when possible, and by binning the results by wind
25   speed.

4.1 Wind-Inflow Characteristics

Many researchers have examined the influence of wind characteristics on turbine load response, considering differing wind parameters and turbulence models, and using different methods to assess their sensitivity. The most common parameter considered is the influence of turbulence intensity variability, which past work has shown to have significant variability and
30   large impact on the turbine response (Dimitrov et al., 2015; Downey, 2006; Eggers et al., 2003; Ernst et al., 2012 Holtslag et al., 2016; Kelly et al., 2014; Matthaus et al., 2017; Moriarty et al., 2002; Rinker, 2016; Saraynsoontorn et al., 2008; Sathe et al., 2012; Sutherland, 2002; Wagner et al., 2010; Walter et al., 2009). The shear exponent, or wind profile, is the next most common parameter examined, concluded to have similar or slightly less importance to the turbulence intensity (Bulaevskaya et al., 2015; Dimitrov et al., 2015; Downey, 2006; Eggers et al., 2006; Ernst et all., 2012; Kelly et al., 2014; Matthaus et al.,
35   2017; Sathe et al., 2012). Other parameters investigated include the turbulence length scale, standard deviation of different directional wind components, Richardson number, spatial coherence, component correlation, and veer. Mixed conclusions are drawn on the importance of these secondary parameters, which are influenced by the range of variability considered (based on the conditions examined), the turbine control system, as well as the turbine size and hub height under consideration. The effects of considering the secondary wind parameters are also mixed, sometimes increasing and sometimes decreasing the loads in
40   the turbine; however, most agree that the use of site-specific measurements of the wind parameters will lead to a more accurate assessment of the turbine loads, resulting in designs that are either better optimized or lower risk.

The focus of this case study is to obtain a thorough assessment of which wind characteristics influence wind turbine structural loads when considering the variability of these parameters over a wide sampling of site conditions.

4.1.1 Parameters

A total of 18 input parameters were chosen to represent the wind-inflow conditions, considering the mean wind profile, velocity spectrum, spatial coherence, and component correlation, as summarized in Table 2. The parameters used were identified considering a Vs model for describing and generating the wind characteristics because it provides a quantitative description with a known and limited set of inputs. Each of these parameters is described in the following sub-sections. Note that the Veers model differs from the other commonly used Mann turbulence model.[1] Regardless, the Veers model is used here because it is more tailorable than the Mann model, *i.e.*, there are more input parameters that can be varied.

Table 2. Wind-inflow condition parameters (18 total).

Mean Wind Profile	Velocity Spectrum	Spatial Coherence	Component Correlation
Shear (σ)	Standard deviation (σ_u, σ_v, σ_w)	Input coherence decrement (a_u, a_v, a_w)	Reynolds stress (PC_{uw}, PC_{uv}, PC_{vw})
Veer (β)	Integral scale parameter (L_u, L_v, L_w)	Offset parameter (b_u, b_v, b_w)	
		Exponent (γ)	

4.1.1.1 Mean Wind Profile

A standard power-law shear model is used to describe the vertical wind speed profile and a linear wind direction veer model is used. The sensitivity of these characteristics are captured through variation of the exponent of the shear, α, and the total veer across the turbine, β (centered around the hub, following right-hand-rule about the vertical axis of the turbine). The IEC 61400-1 standard (IEC, 2005) uses $\alpha = 0.2$ and $\beta = 0°$ under normal turbulence.

4.1.1.2 Velocity Spectrum

The Veers model uses a Kaimal spectrum to represent the turbulence. The Kaimal spectrum is defined as (IEC, 2005):

$$\frac{fS_q(f)}{\sigma_q^2} = \frac{4fL_q/V_{hub}}{(1 + 6fL_1/V_{hub})^{5/3}} \tag{7}$$

where f is the frequency, q is the index of the velocity component direction (u, v, w), S_q is the single-sided velocity spectrum, V_{hub} is the mean wind speed at hub height, σ_q is the velocity component standard deviation, and L_q is the velocity component integral scale parameter. The IEC 61400-1 standard (IEC, 2005) uses a wind-speed-dependent standard deviation, i.e., $\sigma_u = 0.14 \times (0.75V_{hub} + 5.6 \text{ m/s})$, and a set scaling between the direction components of the standard deviation and scale parameters, i.e., $\sigma_v = 0.8\sigma_u$; $\sigma_w = 0.8\sigma_u$; $L_u = 8.1 \times (42 \text{ m}) = 340.2 \text{ m}$; $L_v = 2.7 \times (42 \text{ m}) = 113.4 \text{m}$; and $L_w = 0.66 \times (42 \text{ m}) = 27.72 \text{ m}$. However,

---

[1] The Mann turbulence model (also considered in the IEC 61400-1 standard) is based on a three-dimensional tensor representation of the turbulence derived from rapid distoration of isotropic turbulence using a uniform mean velocity shear (Jonkman, 2009). The Mann model considers the three turbulence components as dependent, representing the correlation between the longitudinal and vertical components resulting from the Reynolds stresses. In the IEC 61400-1 standard, the two spectra (Mann and Kaimal) are equated, resulting in three parameters that may be set for the Mann model. However, there is uncertainty in whether the loads resulting from these two different turbulence spectra are truly consistent.

in this study each parameter in (u, v, w) is varied independently. An inverse Fourier transform is applied to the Kaimal spectrum and random phases derived from the turbulence seed to derive a turbulent time series for each of the wind components independently.

4.1.1.3 Spatial Coherence Model

5   The point-to-point spatial coherence (*Coh*) quantifies the frequency-dependent cross-correlation of a single turbulence component at different transverse points in the wind inflow grid. The general coherence model used in TurbSim is defined as:

$$Coh_{q,f} = \exp\left(-a_q \left(\frac{d}{z_m}\right)^\gamma \sqrt{\left(\frac{fd}{V_{hub}}\right)^2 + \left(b_q d\right)^2}\right) \tag{8}$$

where d is the distance between points i and j, z_m is the mean height of the two points (IEC, 2005), and V_{hub} is the mean wind
10   speed at hub height. The variables a_q and b_q are the input coherence decrement and offset parameter, respectively. Note that the use of V_{hub} in the general coherence model is a modification to the standard TurbSim method. The model is based on the IEC coherence model with the added factor $(d/z_m)^\gamma$ – introduced by Solari (1987) – where γ can vary between 0 and 1. The IEC 61400-1 standard (IEC, 2005) does not use the $(d/z_m)^\gamma$ factor and uses $a_u = 12$ and $b_u = 0.12/L_u$. Coherence is not defined in the standard (IEC, 2005) for the transverse wind components v and w.

15   4.1.1.4 Component Correlation Model

The component-to-component correlation (*PC*) quantifies the cross-correlation between directional turbulence components at a single point in space. For example, PC_{uw} quantifies the correlation between the u and w turbulence components at a given point. TurbSim modifies the v- and w-component wind speeds by computing a linear combination of the time series of the three independent wind speed components to obtain the mean Reynolds stresses (PC_{uw}, PC_{uv}, and PC_{vw}) at the hub. Note that
20   because this calculation occurs in the time domain, the velocity spectra of the v- and w-components are somewhat affected by the enforced component correlations. The IEC 61400-1 standard (IEC, 2005) does not specify Reynolds stresses.

4.1.2 Parameter Ranges

To assess the sensitivity of each of the parameters on the load response, a range over which the parameters could vary was defined. The variation level was assessed through a literature search seeking the range over which the parameters could
25   realistically vary for different wind-farm sites around the world (Berg et al., 2013; Bulaevskaya et al., 2015; Clifton; Dimitrov et al., 2016; Dimitrov et al., 2015; Eggers et al., 2003; Ernst et al., 2012; Holtslag et al., 2016; Jonkman, 2009; Kalverla et al., 2017; Kelley, 2011; Lindelöw-Marsden, 2009; Matthaus et al., 2017; Moriarty et al., 2002; Moroz, 2017; Nelson et al., 2003; Park et al., 2015; Rinker, 2016; Saint-Geours et al., 2010; Saranyasontoorn et al., 2004; Saranyasontoorn et al., 2008; Sathe et al., 2012; Solari, 1987; Sutherland, 2002; Teunissen, 1970; Wagner et al., 2010; Walter et al., 2009; Wharton et al., 2015;
30   Ziegler et al., 2016). When possible, parameter ranges were set based on wind speed bins. If no information on wind-speed dependence was found, the same values were used in all bins. The ranges, summarized in Table 3, were taken from multiple sources (references cited below the values), based on measurements across a variety of different locations and conditions. For comparison, the nominal value prescribed by IEC for category B turbulence is specific in the "Nom" row.

35   To simplify the screening of the most influential parameters, all parameters were considered independent of one another. This was done because of the difficulty of considering correlations between a large number of parameters. Such correlations should be studied in future work once parameter importance has been established. Since each parameter was considered independently, except for the conditioning on wind speed bin, some non-physical parameter combinations may arise. This was considered acceptable for the screening process.

4.1.3 Elementary Effects

The EE value was calculated for each of the 18 input parameters (I) at 30 different starting points (R) in the input-parameter hyperspace. The number of points was determined through a convergence study on the average of the EE value. At each of the points examined, S different turbulent wind files (i.e. S independent time-domain realizations from S seeds) were run. Thirty seeds were needed based on a convergence study of the ultimate and fatigue load metrics for all QoIs. Based on these numbers, the total number of simulations performed for the wind-inflow case study was $R \times (I+1) \times S \times B = 30 \times 19 \times 30 \times 3 = 51,300$, where B is the number of wind speed bins considered.

The EE values across all input parameters, input hyperspace points, and wind speed bins were examined for each of the QoIs for ultimate and fatigue loads. To identify the most sensitive parameters, a tally was made of the number of times an EE value exceeded the threshold for a given QoI. The resulting tallies are shown in Figure 3, with the ultimate load tally on the left and the fatigue load tally on the right. As expected, these plots show an overwhelming level of sensitivity of the u-direction turbulence standard deviation (σ_u) and also the vertical wind shear (α). However, focusing on the lower tally values in this plot highlights the secondary-level of importance of veer (β), u-direction integral length (L_u) and components of the IEC coherence model (a_u and b_u), as well as the exponent (γ).

Table 3: Included wind-inflow parameter ranges separated by wind speed bin.

	α (-)	β (deg)	L_u (m)	L_v (m)	L_w (m)	σ_u (m/s)	σ_v (m/s)	σ_w (m/s)	a_u (-)	a_v (-)	a_w (-)	b_u (m⁻¹)	b_v (m⁻¹)	b_w (m⁻¹)	γ (-)	PC_{uw} (m²/s²)	PC_{uv} (m²/s²)	PC_{vw} (m²/s²)
Below-rated wind speed, 3-10 m/s																		
Nom.	0.2	0	340	110	28	1.6	1.3	1.3	12	-	-	3.5E-4	-	-	0	-	-	-
Min.	-1.5*	-25	5	2	2	0.05	0.02	0.03	1.5	1.7	2	0	0	0	0	-3.5	-4.5	-2.7
Max.	3.3	50	1,000	1,000	650	7.2	7.4	4.5	26	18	17	0.08	4.5E-3	0.011	1	0.50	6.0	1.0
Ref.	Clifton	Walter et al., 2009	Nelson et al., 2003; Solari et al., 2001	Nelson et al., 2003	Nelson et al., 2003; Teunissen, 1970	Clifton	Clifton	Clifton	Solari 1987	Saranyasoontorn et al., 2006	Solari 1987 Solari et al., 2001	Saranyasoontorn et al., 2004	Jonkman 2009	Jonkman 2009	Solari 1987	Kelley 2011	Kelley 2011	Kelley 2011
Near-rated wind speed, 10-14 m/s																		
Nom.	0.2	0	340	110	28	2.0	1.6	1.6	12	-	-	3.5E-4	-	-	0	-	-	-
Min.	-0.4	-10	8	2	2	0.20	0.05	0.05	1.5	1.7	2	0	0	0	0	-3.5	-4.5	-2.7
Max.	0.9	50	1,400	1,300	450	7.3	8.1	4.3	26	18	17	0.08	3.0E-3	6.0E-3	1	0.50	6.0	1.0
Ref.	Dimitrov et al., 2015; Moroz 2017	Dimitrov et al., 2015; Walter et al., 2009	Nelson et al., 2003; Solari et al., 2001	Nelson et al., 2003	Nelson et al., 2003	Clifton; Kelley 2011	Clifton; Kelley 2011	Clifton; Kelley 2011; Nelson et al., 2003	Solari 1987	Saranyasoontorn et al., 2006	Saranyasoontorn et al., 2006; Solari 1987	Saranyasoontorn et al., 2004	Jonkman 2009	Jonkman 2009	Solari 1987	Kelley 2011	Kelley 2011	Kelley 2011
Above-rated wind speed, 14-25 m/s																		
Nom.	0.2	0	340	110	28	2.7	2.1	2.1	12	-	-	3.5E-4	-	-	0	-	-	-
Min.	-0.4	-10	25	2	2	0.20	0.18	0.15	1.5	1.7	2	0	0	0	0	-3.5	-4.5	-2.7
Max.	0.7	25	1,600	1,500	650	7.4	7.3	4.2	26	18	18	0.05	2.5E-3	6.5E-3	1	0.50	6.0	1.0
Ref.	Dimitrov et al., 2015; Moroz 2017	Dimitrov et al., 2015; Walter et al., 2009	Kelly et al., 2014; Nelson et al., 2003	Nelson et al., 2003	Nelson et al., 2003	Clifton Kelley 2011; Nelson et al., 2003	Clifton Kelley 2011; Nelson et al., 2003	Clifton Kelley 2011;	Solari 1987	Saranyasoontorn et al., 2006	Jonkman 2009; Solari et al., 2001	Saranyasoontorn et al., 2004	Jonkman 2009	Jonkman 2009	Solari 1987	Kelley 2011	Kelley 2011	Kelley 2011

* This value was changed to -0.75 due to simulation issues
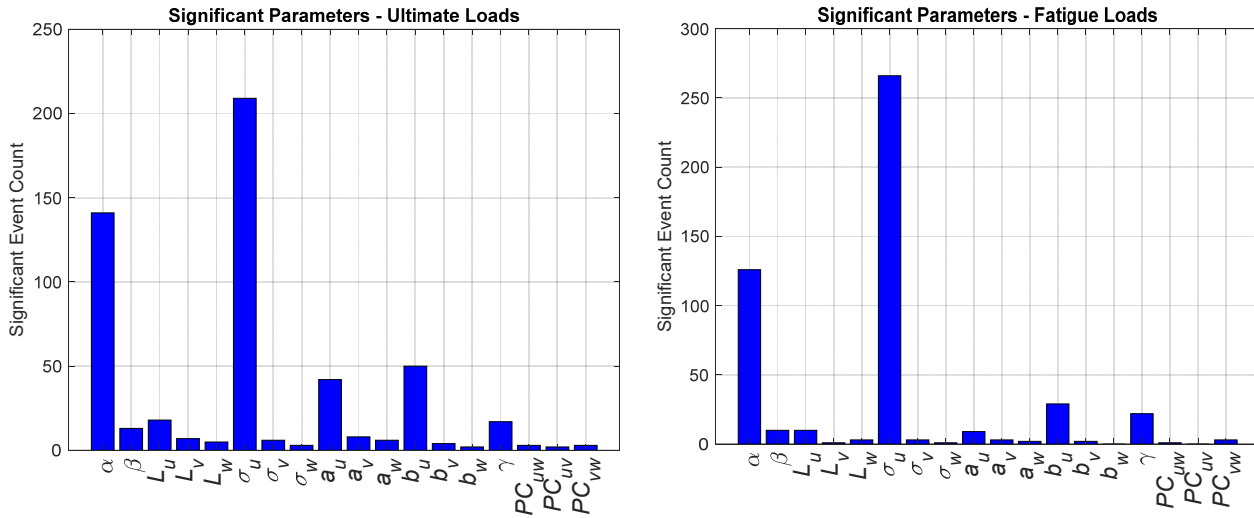
Figure 3: Identification of significant parameters using ultimate (left) and fatigue (right) loads. Significant events are defined by number of outliers identified across each of the QoIs for all wind speed bins, input parameters, and simulation points.

Histograms of the EE values for each of the QoIs are plotted in Figure 4 and Figure 5 for the ultimate and fatigue load metrics (associated exceedance probability plots are shown in Appendix B, Figure 21 and Figure 22). Each plot contains all calculated EE values for a given QoI colored by wind speed bin. The threshold used to identify significant EE values is shown in each plot as a solid black line. All points above the threshold line indicate a significant event and are included in the outlier tally for each QoI. Note that while electric power is shown, it is not used in the outlier tally because its variation is strictly limited by the turbine controller rather than other wind parameters. Highlighted in these figures is that most of the outliers come from the below-rated wind speed bin.

To understand why the below-rated wind speed bin would be creating the most outliers, a more thorough examination is made for one of the QoIs. Exceedance probability plots of blade-root loads are shown in Figure 6. Here, all input parameters are plotted independently of each other to compare the behavior between parameters. Each line represents a different input parameter, with each point representing a different location in the hyperspace. These plots show how the shear and u-component standard for the lower wind speed bin stand-out compared to all other parameters; likewise, the u-component standard deviation stands out across different wind speed bins for the ultimate load. One of the reasons that the shear value shows such a large sensitivity in the lowest wind speed bin is the large range over which the parameter is varied. A smaller range is used for the near- and above-rated bins, resulting in less sensitivity to shear for those wind speeds. The impact of the range on the sensitivity of the parameter indicates that for sites with extreme conditions, such as an extreme shear, using appropriate parameter values in a loads analysis can be important in accurately assessing the ultimate and fatigue loading on the turbine. The effect of shear could also be diminished by employing independent blade-pitch control, whereas the reference NREL 5-MW turbine controller used here employs collective blade-pitch control.

Histogram plots of blade-root bending moment EE values are shown in Figure 7 and Figure 8. In each figure, wind speed bins are displayed in different plots and EE value histograms showing the contribution from all input parameters are shown in each histogram. Ultimate load EE values are shown in Figure 7 and fatigue load EE values are shown in Figure 8. Highlighted in these plots is the large sensitivity of the shear parameter and, to a lesser extent, u-component standard deviation in the far extremes.
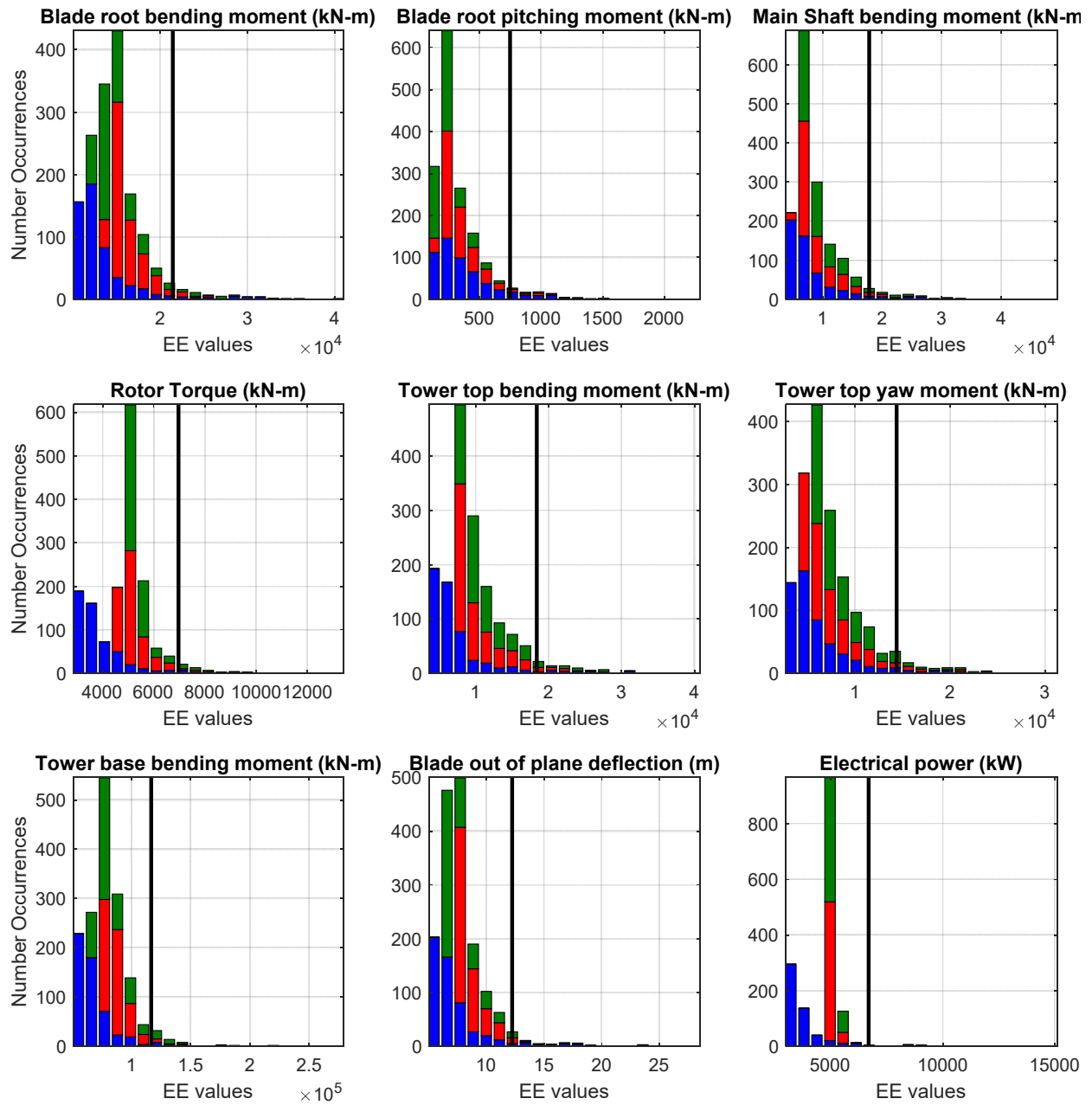
Figure 4: Stacked histogram of the ultimate load EE values for each of the QoIs across all wind speed bins, input parameters, and simulation points. Black line represents the defined threshold by which outliers are counted for each QoI. Color indicates wind speed bin (blue=below rated, red=near rated, green=above rated).
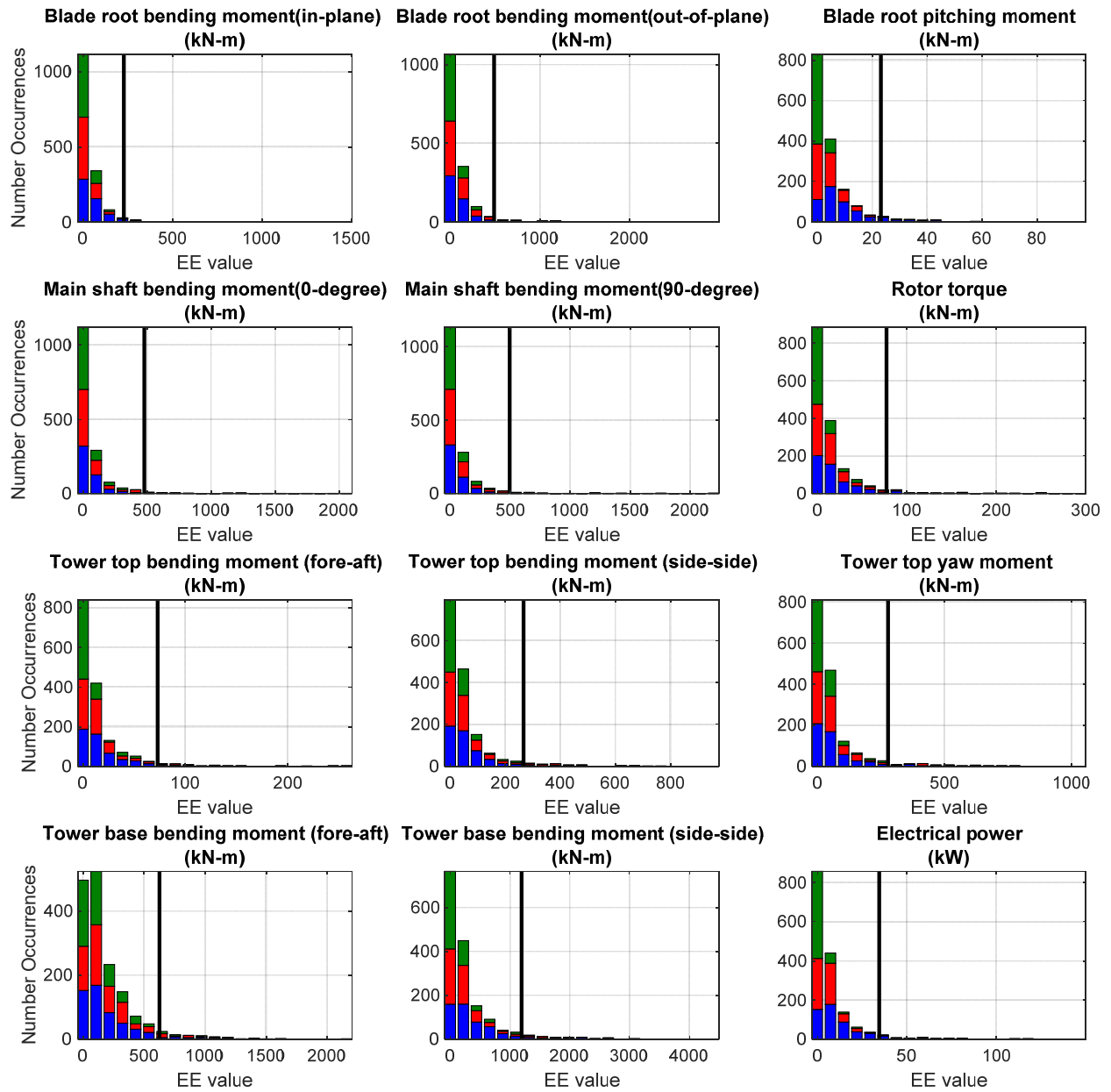
Figure 5: Stacked histogram of the fatigue load EE values for each of the QoIs across all wind speed bins, input parameters, and simulation points. Black line represents the defined threshold by which outliers are counted for each QoI. Color indicates wind speed bin (blue=below rated, red=near rated, green=above rated).
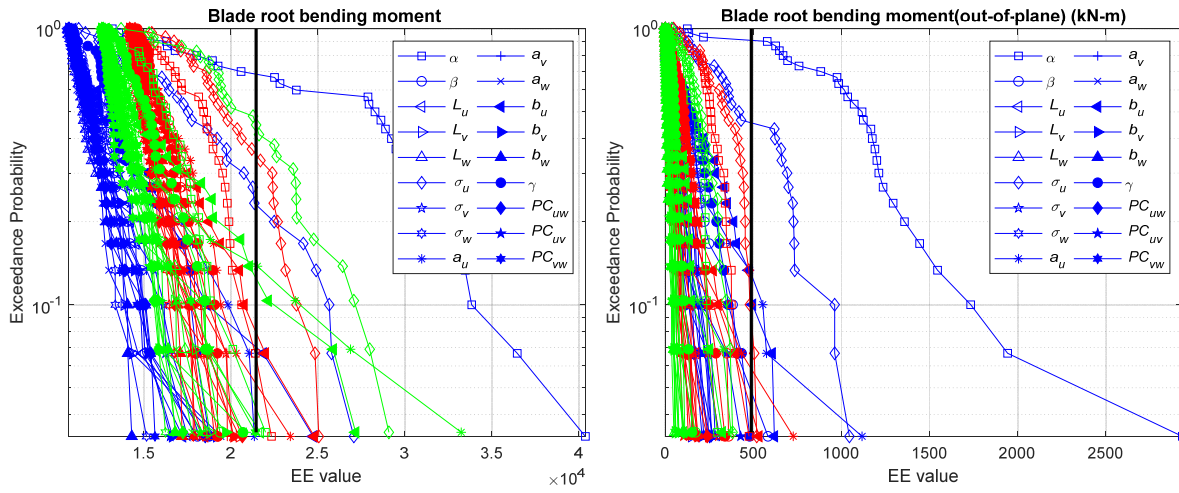
Figure 6: Exceedance probability plot of ultimate (left) and fatigue (right) load EE values for blade-root bending moments. Each line represents a different input parameter and wind speed bin (blue=below rated, red=near rated, green=above rated).
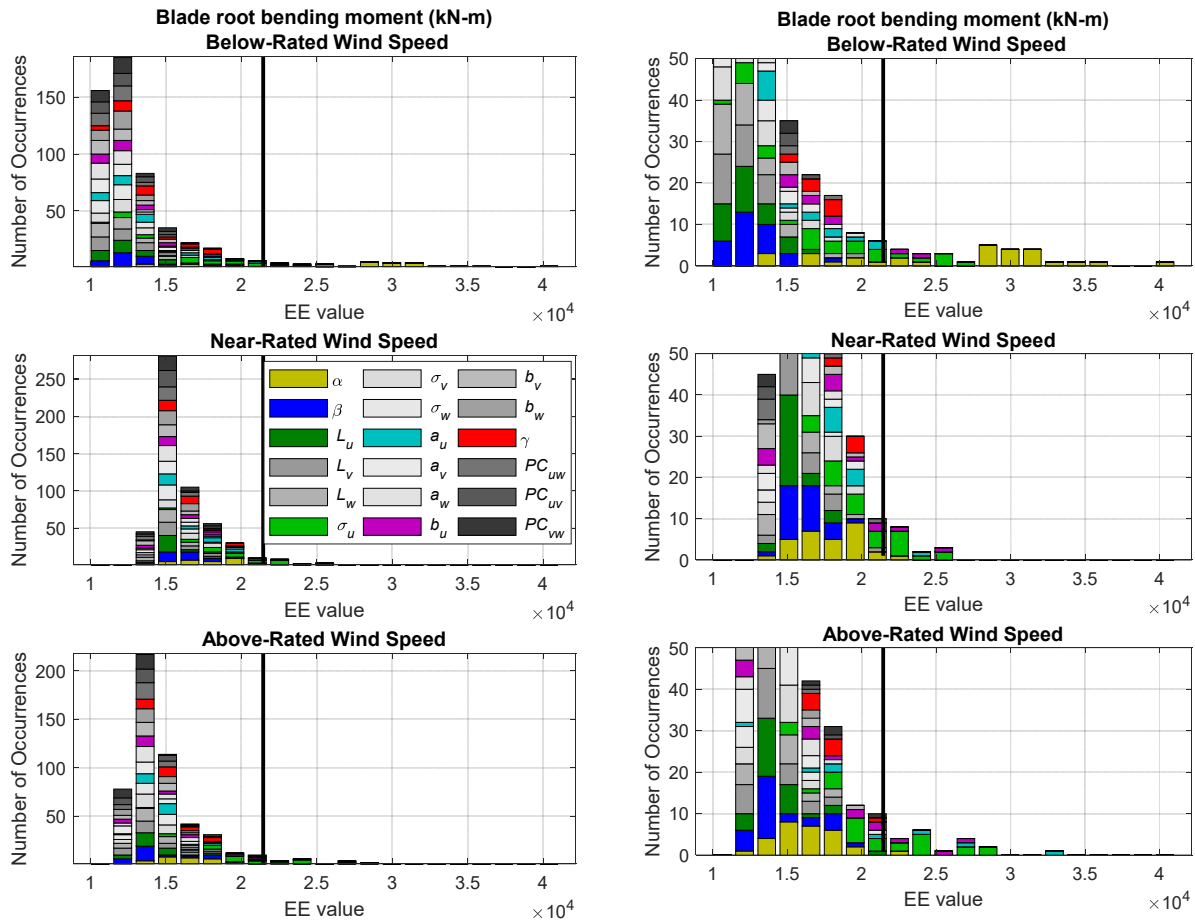
Figure 7: Histogram of ultimate load EE values for the blade-root bending moment. Each graph (in left column) shows one wind speed bin and includes all input parameters. Right column is a zoom of the left.
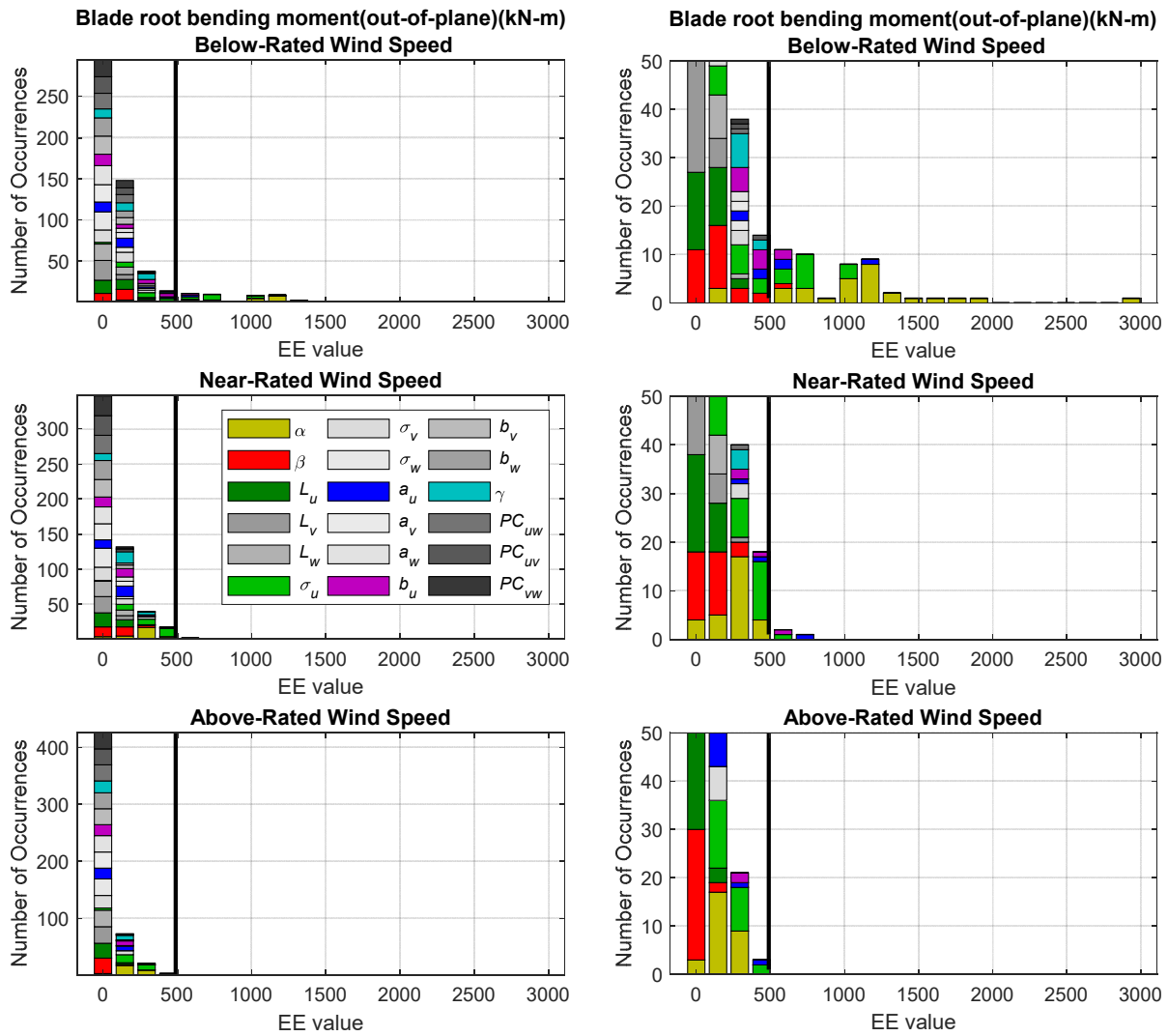
Figure 8: Histogram of fatigue load EE values for the blade-root bending out-of-plane bending moment. Each graph (in left column) shows one wind speed bin and includes all input parameters. Right column is a zoom of the left.

To summarize which parameters are important for which QoIs, the number of times each input parameter contributed to the significant event count for a given QoI was tallied. The top most sensitive parameters are shown in Table 4 and Table 5 for ultimate and fatigue loads, respectively. Overall, 46% of the outliers for both ultimate and fatigue loads are due to u-direction turbulence standard deviation (σ_u), and 26% for vertical shear (α), and for all but two QoIs, these are the most sensitive parameters. The two exceptions are blade-root pitching moment and tower-base bending moment, which show u-direction turbulence standard deviation as the most important parameter, but show coherence properties and integral scale parameter as more important than shear. This is understandable since shear will have little effect on collective blade pitching and rotor thrust. The remaining parameters have far less significance, with only components of the IEC coherence model, a_u (5%) and b_u (8%), having a value great than 1%. These results can be used in future sensitivity analysis work to focus on perturbation of specific input parameters based on desired turbine loads.

Table 4. Top input parameters contributing to ultimate load sensitivity of each QoI. Values indicate how many times the variable contributes to the sensitivity count.

Blade-Root Bending Mom.	Blade-Root Pitch Mom.	Main Shaft Bending Mom.	Rotor Torque	Tower-Top Bending Mom.	Tower-Top Yaw Mom.	Tower-Base Bending Mom.	Blade OoP Deflection
σ_u (29)	σ_u (26)	α (33)	σ_u (28)	α (31)	σ_u (41)	σ_u (22)	α (22)
α (22)	γ (10)	σ_u (28)	α (12)	σ_u (22)	α (10)	a_u, b_u, L_u (8)	σ_u (13)
b_u (7)	L_u (8)	a_u, b_u (5)	b_u (6)	a_u, b_u (5)	a_u, b_u (8)	--	b_u (9)

Table 5. Top input parameters contributing to fatigue load sensitivity of each QoI. Values indicate how many times the variable contributes to the sensitivity count.

Blade-Root IP Bend. Moment	Blade-Root OP Pitch. Moment	Blade-Root Pitch. Moment	Main Shaft Bending Moment 0°	Main Shaft Bending Mom. 90°	Rotor Torque	Tower-Top FA Bend. Moment	Tower-Top SS Bend. Moment	Tower-Top Yaw Moment	Tower-Base FA Bend. Moment	Tower-Base SS Bend. Moment
σ_u (10)	α (14)	σ_u (14)	α (18)	α (18)	σ_u (25)	σ_u (31)	σ_u (47)	σ_u (48)	σ_u (24)	σ_u (35)
α (8)	σ_u (9)	L_u (7)	σ_u (12)	σ_u (11)	α (11)	α (12)	α (13)	α (12)	α (6)	α (9)
b_u (3)	b_u (4)	α (5)	β (2)	β (2)	b_u (9)	b_u (7)	γ (3)	γ (3)	γ (4)	γ (4)

4.2 Aeroelastic Turbine Properties

The second case study focuses on which aeroelastic turbine parameters have the greatest influence on turbine ultimate and fatigue loads during normal turbine operation. These properties are categorized into four main categories: support structure, blade structural, blade aerodynamic, and controller properties.

It is widely acknowledged that uncertainty in the aerodynamic parameters can affect the prediction of turbine performance and structural loading (Abdallah et al., 2015; Madsen et al., 2010; Simms et al, 2001). Abdallah et al. (2015) demonstrated the impact of uncertainty in steady airfoil data on prediction of extreme loads and assessed the correlation between various static coefficient polars (Abdallah et al., 2015). Despite significant work to measure these parameters, considerable uncertainty remains in their prediction. Static lift and drag measurements almost exclusively come from wind tunnel tests of airfoils, which lack three-dimensional and unsteady effects that are instead estimated through the application of semi-empirical engineering models, e.g., rotational augmentation (stall delay) and stall hysteresis (Abdallah et al., 2015, Simms et al, 2001). In Damiani (2010), unsteady aerodynamic parameters were tuned for several airfoil sections to match experimental lift and drag unsteady hysteresis loops, but the consequences of parameter variation were not considered. Blade chord and twist ranges were chosen using the work of Loeven and Bihl (2008), who identified changes in blade chord and twist based on uncertainty in aerodynamic loading, icing, or wear of the blades.

Beyond the blade aerodynamic properties, other turbine properties also contribute to the uncertainty of the load response characteristics. Abdallah (2015) provides a comprehensive assessment of the sources of uncertainty affecting the prediction of loads in a wind turbine. Researchers have not focused on these other parameters as significantly as the aerodynamic ones, but they could have a significant contribution to the uncertainty. Witcher (2017) examined uncertainty in properties such as the tower and blade mass/stiffness properties within the context of defining a probabilistic approach to designing wind turbines by examining distributions of the load from propagated input parameter uncertainties versus resistance distributions. Prediction of the reliability of the wind turbine has been studied through examination of the damping in the structure by Koukoura (2014) and a better understanding of the uncertainty in the properties of the drivetrain by Holierhoek (2010). Limited information is available on what the actual ranges of uncertainty are for these different characteristics. For most studies, expert opinion is used to set a realistic bound. A better assessment of these bounds will be needed in future work to understand the relative importance of the physical parameters and to provide a more precise assessment of the uncertainty bounds in the load response of wind turbines.

4.2.1 Parameters

For the turbine aeroelastic properties, 39 input parameters were identified covering support structure properties, blade structural properties, blade aerodynamic properties (both steady and unsteady characteristics), and controller properties. These parameters are summarized in (acronyms are defined in the following subsections).

Table 6. Turbine aeroelastic parameters (39 total).

Support Structure Properties	Blade Structural Properties	Blade Aerodynamic Properties	Controller Properties
Nacelle mass (N_{Mass})	Blade flapwise stiffness (B_{FK})	Twist (ø) at tip	Yaw Angle Error (θ)
Nacelle CM x-location (N_{CM})	Blade edgewise stiffness (B_{EK})	Chord (c) at root and tip	Collective pitch error ($ø_{err,coll}$)
Tower CM location (T_{CM})	Blade flapwise stiffness imbalance ($B_{FK,imb}$)	Leading-edge separation time constant (T_{f0})	Imbalanced pitch error ($ø_{err,imb}$)
Tower stiffness (T_{KF})	Blade edgewise stiffness imbalance ($B_{EK,imb}$)	Vortex shedding time constant (T_{V0})	
Tower mass (T_{MD})	Blade damping ratio (B_{DR})	Leading-edge pressure gradient time constant (T_p)	
Tower damping ratio (T_{DR})	Blade mass (B_M)	Vortex advection time constant (T_{VL})	
Drivetrain stiffness (D_K)	Blade mass imbalance ($B_{M,imb}$)	Strouhal Number (St_{sh})	
Drivetrain damping (D_D)	Blade CM location (B_{CM})	Lift (C_l) at root and tip	
Shaft angle (α_S)	Precone (β_p)	TES Lift AoA (α_{TES}) at root and tip	
		Max Lift AoA (α_{max}) at root and tip	
		SR Lift AoA (α_{SR}) at root and tip	
		0-degree drag ($C_{d,0}$) at root and tip	

4.2.2 Parameter Ranges

The level of variation was based on the perceived level of uncertainty in the parameter values. Some of these levels of uncertainty are proposed within the literature, but when no other information was available, expert opinion was used. The source for the information is provided below the values in each table summarizing the parameter ranges. "Exp" is used to identify where expert opinion was used. The uncertainty levels are largely percentage based, but in some instances an exact value was used. The following sub-sections define the ranges of the parameters introduced in Table 6. All parameters were considered independent of one another, as was done for the wind parameter sensitivity analysis.

4.2.2.1 Support Structure Properties

For the support structure, 9 parameters were varied and summarized in Table 6. These parameters included mass and center of mass (CM) of the tower and nacelle; tower and drivetrain stiffness factors; tower and drivetrain damping ratio; and shaft angle. To manipulate the tower structural response, the frequency of the corresponding tower mode shapes was changed by ±15% of

0.32 Hz by uniformly scaling the associated stiffness. While tower stiffness is specified as a factor by which mode shapes are scaled, the drivetrain stiffness is entered directly. Note that the mode shapes themselves (which are specified independently of the mass and stiffness in ElastoDyn) were not changed in this process. The tower mass was changed by varying the distributed tower mass density factory. The tower CM location was changed by varying the tower-base and -top density such that density increased at one end and decreased at the other without changing the overall blade mass. The drivetrain damping term represents the combined effect of structural damping and drivetrain damping from active control.

Table 7: Parameter value ranges of turbine support structure parameter ranges.

	N_{mass} (kg)	N_{CM} (m)	T_{CM} (m)	T_{KF} (-)	T_{MD} (-)	T_{DR} (%)	D_K $\left(\frac{N \bullet m}{rad}\right)$	D_D $\left(\frac{N \bullet m}{rad/sec}\right)$	α_S (deg)
Nom.	240,000	1.9	42.505	1.02	1	2.55	867,637,000	6,215,000	-5
Min.	216,000	1.71	40.38	0.72	0.95	0.1	780,873,300	0.0	-5.2
Max.	264,000	2.09	44.63	1.32	1.05	5.0	954,400,700	12,430,000	-4.8
Ref.	Witcher, 2017	Exp	Exp	Koukoura 2014	Witcher, 2017	Koukoura 2014	Holierhoek et al., 2010	Holierhoek et al., 2010	Santos and van Dam, 2015

4.2.2.2 Blade Structural Properties

For the blade structural properties, 9 parameters were considered, including blade flapwise and edgewise stiffness (including stiffness imbalance), mass (including mass imbalance), CM, damping, and precone angle, as detailed in Table 8. Through ElastoDyn, blade structural dynamics are modeled using two flapwise mode shapes and one edgewise mode shape per blade. To manipulate blade structural response, the frequency of the flapwise and edgewise mode shapes was changed by ±5% of 0.7 Hz and 1 Hz, respectively, by uniformly scaling the associated stiffness. The blade mass was changed by uniformly scaling the distributed blade mass of all blades. The nominal scaling of 1.04536 is described in the NREL 5-MW specifications document (Jonkman et al., 2009). The blade CM location was changed by varying the blade root and tip density such that density increased at one end and decreased at the other without changing the overall blade mass. Blade imbalance effects were also included by varying the mode frequency and mass of each blade. The imbalances were introduced by applying a different change value to each blade. Specifically, one blade is modified to be a value that is higher than the nominal value, and another modified to a lower value. The third blade remains unchanged at the nominal value.

Table 8: Parameter value ranges of turbine blade structure parameter ranges.

	B_{FK} (-)	B_{EK} (-)	$B_{FK,imb}$ (-)	$B_{EK,imb}$ (-)	B_{DR} ($\%_{critical}$)	B_M (-)	$B_{M,imb}$ (-)	B_{CM} (m)	β_p (deg)
Nom.	1	1	0.01	0.01	1.55	1.04536	0.025	0.015	-2.5
Min.	0.9	0.9	0.0	0.0	0.1	0.993	0.0	20.60	-2.75
Max.	1.1	1.1	0.02	0.02	3.0	1.1	0.05	22.60	-2.25
Ref.	Exp	Exp	Exp	Exp	Exp	Witcher, 2017	Exp	IEC, 2010	Exp

4.2.2.3 Blade Aerodynamic Properties

The blade aerodynamic properties were represented using 18 parameters: 3 associated with blade twist and chord distribution; 10 associated with the static aerodynamic component; and 5 associated with the unsteady aerodynamic properties.
Blade twist and chord distributions were manipulated by specifying a change in the distributions along the blade. Three parameters were defined, associated with changing the chord at the blade tip and root, and the twist at the blade tip. For each of these parameters, the associated distribution along the blade was modified linearly such that there was zero change at the opposite end. The root twist was not changed because the blade-pitch angle uncertainties are considered in the controller parameter section.

4.2.2.4 Steady Airfoil Aerodynamics

For the steady aerodynamic component, the lift and drag versus angle-of-attack (AoA) curves were modified to examine the sensitivity on resulting loads throughout the wind turbine. The turbine operated in normal operating conditions, and therefore only relevant regions of the curves were modified. To modify the curves, the curves were parameterized using an approach based on one introduced by Abdallah et al. (2015). The approach used here parameterizes the C_l and C_d curves using five points; these points were perturbed and a spline fit to the points. The points of interest are:

- Beginning of linear C_l region — determines the lower limit of the AoA range of interest and was kept constant (α_{lin}, $C_{l,lin}$);
- C_d value at AoA = 0° (0°, $C_{d,0}$);
- Trailing edge separation (TES) point — AoA location at which C_l curve is no longer linear (α_{TES}, $C_{l,TES}$);
- Maximum (max) point – AoA location at which C_l reaches a maximum (α_{max}, $C_{l,max}$);
- Separation reattachment (SR) point — AoA location at which slope of C_l curve is no longer negative (α_{SR}, $C_{l,SR}$).

The selected points of interest are similar to those selected by Abdallah et al. (2015). A notable difference is the consideration of $C_{d,0}$ as opposed to $C_{d,90}$, which is the C_d value at $\alpha=90°$. $C_{d,0}$ was chosen for this study because of the focus on normal operational region, as opposed to the extreme conditions considered by Abdallah et al. (2015). The three variable points of interest were perturbed by a percentage of the default value. The perturbations and correlations are depicted in Figure 9 and parameter ranges are detailed in Table 9. From Abdallah (2015), the TES, max, and SR C_l values for an individual airfoil have
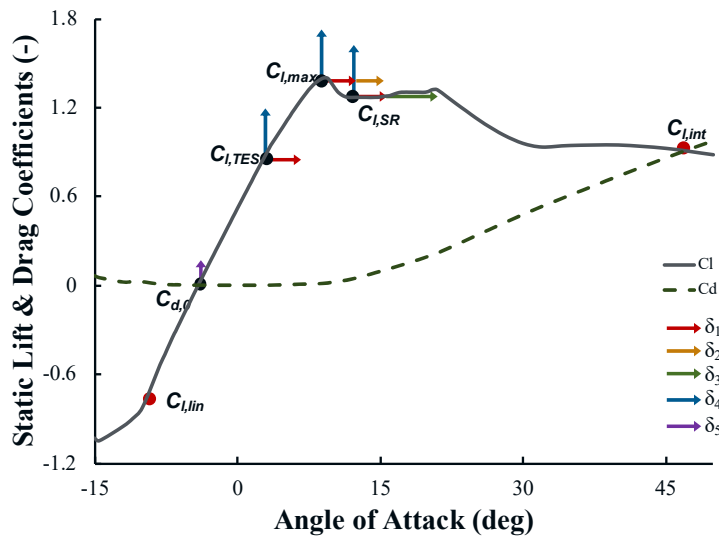
Figure 9: Perturbation of points of interest in representative C_l and C_d curves.

a correlation to one another of 0.9. Thus, all C_l values are perturbed collectively, using the same percentage (δ_4). The AoA values are less correlated and are therefore perturbed independently of one another. However, to ensure that nonphysical relative values are not reached, all AoA values are perturbed by the same base percentage (δ_1), and then an additional independent variation of a smaller value was added (δ_2 and δ_3) for α_{max} and α_{SR}, respectively. The $C_{d,0}$ value was also perturbed (δ_5).

C_l and C_d curves were altered for each airfoil. However, instead of specifying δ values for each airfoil, these values were specified at the root and tip airfoils, excluding the cylindrical airfoils at the base. Perturbation values for the interior airfoils

were computed from a linear fit of the endpoint values. The method of developing the new curves for each airfoil is detailed here:

1. AoA deltas are applied to the original AoA values via the following equations:

$$\alpha_{\text{TES,new}} = \alpha_{\text{TES,orig}} + \alpha_{\text{TES,orig}}\delta_1 \tag{8}$$
$$\alpha_{\text{max,new}} = \alpha_{\text{max,orig}} + \alpha_{\text{max,orig}}(\delta_1 + \delta_2) \tag{9}$$
$$\alpha_{\text{SR,new}} = \alpha_{\text{SR,orig}} + \alpha_{\text{SR,orig}}(\delta_1 + \delta_3) \tag{10}$$

2. The new AoA values are fit to the nearest existing AoA value on the curve. The AoA resolution is fine enough that all perturbations are captured, though not precisely. This approach may need to be adjusted if the perturbations were to decrease.

3. For all new AoA values, the change in C_l between the original C_l value ($C_{l,\text{TES}}$) and the C_l curve value at the new AoA ($C_{l,\text{orig+}}$) is computed via:

$$\epsilon = C_{l,\text{orig+}} - C_{l,\text{orig}}$$

4. The total change in C_l is then computed via:

$$C_{l,\text{diff}} = \delta_4 C_{l,\text{orig}} - \epsilon$$

This ensures that if $\delta_4 = 0$, the final $C_{l,\text{new}}$ value is equivalent to that of the original curve.

5. For C_l perturbation, the end points are located at the AoA associated with the beginning of the linear C_l region ($C_{l,\text{lin}}$) and $\alpha = 90°$; as these are fixed points, they have $C_{l,\text{diff}} = 0$. The C_l curve is replaced by a line between (α_{lin}, $C_{l,\text{lin}}$) and (α_{TES}, $\delta_4 C_{l,\text{lin}}$). A piece-wise linear spline – representing perturbations about the original curve – is constructed between the points ($\alpha_{\text{TES,new}}$, $\delta_4 C_{l,\text{TES}}$); ($\alpha_{\text{max,new}}$, δ_4,$C_{l,\text{max}}$); ($\alpha_{\text{SR,new}}$, δ_4,$C_{l,\text{SR}}$); and (90°, 0).

6. The $C_{l,\text{diff}}$ values calculated from the spline fit are added to the original C_l curve.

$$C_{l,\text{new}} = C_{l,\text{orig+}} + C_{l,\text{diff}}$$

A similar process was followed by modifying the C_d curves, wherein the C_d value corresponding to $\alpha = 0°$ ($C_{d,0}$) is perturbed by a specified value (δ_5) in the same manner as the C_l values. A piece-wise linear spline is then fit between (-90°, $C_{d,-90}$), (0°, $C_{d,0}$), and (90°, $C_{d,90}$) and added to the original C_d curve. $C_{d,0}$ is constrained to not go below 0. Several modified C_l and C_d curves for each airfoil section are shown in Figure 10. Note that C_d curves are perturbed, but by a very small amount not visible in the plots. These perturbations result in modified C_l and C_d curves that maintain the primary characteristics of the original curve, but differ in both magnitude and feature location.

4.2.2.5 Unsteady Airfoil Aerodynamics

There are several unsteady airfoil aerodynamic parameters that can be modified in OpenFAST. By expert opinion (Damiani, 2018), several of these parameters have been identified as having the largest potential variability or impact on turbine response and are therefore included in this study. Several of the parameters in the Beddoes-Leishman-type unsteady airfoil aerodynamics model used here are derivable from the (perturbed) static lift and drag polars, i.e., when the lift and drag polars are perturbed, the associated Beddoes-Leishman unsteady airfoil aerodynamic parameters are perturbed as well. Additionally, there are several other parameters associated with unsteady aerodynamics that are included in OpenFAST. These parameters are:

- T_{f0} — time constant connected to leading-edge separation of the airfoil;
- T_{V0} — time constant connected to vortex shedding;
- T_p — time constant connected to the leading-edge pressure gradient;
- T_{VL} — time constant connected to the vortex advection process;
- St_{sh} — Strouhal number associated with the vortex shedding frequency.

These quantities were varied over the ranges detailed in Table 9 and are constant across the blade.

Table 9: Parameter value ranges of turbine blade aerodynamic parameter ranges.

	$\emptyset_{tip}$ (deg)	c_r (m)	c_t (m)	T_{f0} (-)	T_{V0} (-)	T_p (-)	T_{VL} (-)	St_{sh} (-)	$C_{l,tr}$ (-)	$\alpha_{TES,tr}$ (deg)	$\alpha_{max,tr}$ (deg)	$\alpha_{SR,tr}$ (deg)	$C_{d,0,tr}$ (-)
Nom.	0.106	3.542	1.419	6.5	8	1.35	16.5	0.245	Var.	Var.	Var.	Var.	Var.
Min.	-1.894	3.1878	1.2771	3	1	1	11	0.19	-26%	-20%	-8%	-15%	-100%
Max.	2.106	3.8962	1.5609	10	15	1.7	22	0.3	+26%	+20%	+8%	+15%	+100%
Ref.	Petrone et al., 2011	Loeven and Bijl, 2008	Loeven and Bijl, 2008	Damiani et al., 2016	Damiani et al., 2016	Damiani et al., 2016	Damiani et al., 2016	Damiani et al., 2016	Abdallah et al., 2015	Abdallah et al., 2015	Abdallah et al., 2015	Abdallah et al., 2015	Ehrmann et al., 2017
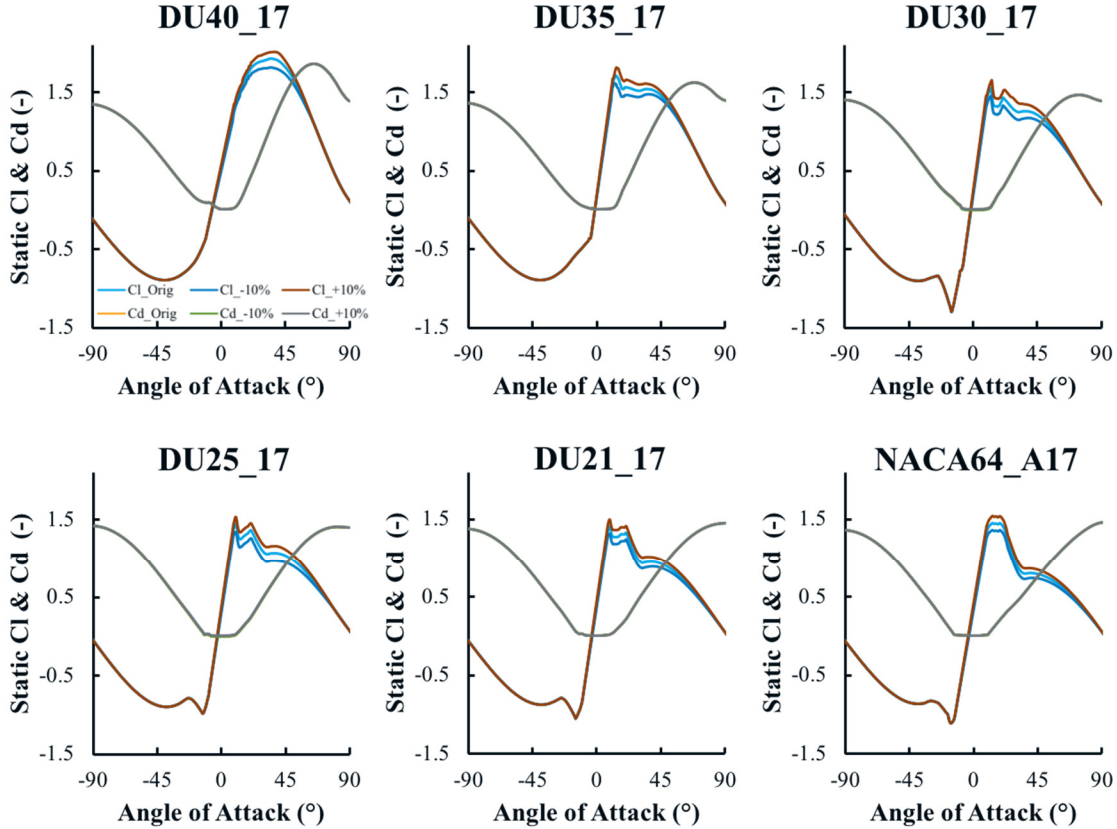
Figure 10: Sample original and perturbed C_l and C_d curves for each airfoil section used in the NREL 5-MW reference turbine.
Perturbed values represent ±10% of the specified range for each parameter.

4.2.2.6 Controller Properties

Turbine yaw error was incorporated by directly changing the yaw angle of the turbine (see Table 10). For the collective blade pitch error, the twist distribution of each blade is identically shifted uniformly along the blade independent of the twist change in Table 9. For the imbalance pitch error, modified twist distributions are applied to two of the blades: one with a higher-than-nominal tip twist, one with a lower-than-nominal tip twist, and one unchanged.

Table 10: Parameter value ranges of turbine controller parameter ranges.

	θ (deg)	$\emptyset_{err,coll}$ (deg)	$\emptyset_{err,imb}$ (deg)
Nom.	0	0	0.1
Min.	-20	-0.2	0
Max.	20	0.2	0.2
Ref.	Quick et al., 2017	Simms et al., 2001	Simms et al., 2001

4.3 Elementary Effects

The EE value calculation and analysis process are the same as was used for the wind parameter analysis. 60 wind file seeds were needed based on a convergence study of the ultimate and fatigue load metrics for all QoIs. This increase in the number in required wind file seeds over the other study is likely due to some turbine input parameter combinations causing resonance. Based on these numbers, the total number of simulations performed for the wind-inflow case study was R×(I+1)×S×B = 30×40×60×3 = 216,000.

The EE values across all input parameters, input hyperspace points, and wind speed bins were examined for all QoI for the ultimate and fatigue loads. For each QoI, the number of times an EE value exceeded the threshold for a given QoI was tallied. The resulting tallies are shown in Figure 11, with the ultimate load tally on the top and fatigue load tally on the bottom. Note that nearly twice as many significant events were counted for fatigue loads; less significant events were counted for ultimate loads because of the limited threshold exceedance in the below-rated wind speeds. The percentage that each relevant input parameter contributed to the total significant event count is summarized in Table 11. Ultimate turbine loads are most sensitive to yaw error (θ) and C_1 distribution at the outboard section of the blade ($C_{1,t}$), which combined accounted for nearly half of all significant events. Fatigue loads are also highly sensitive to blade mass imbalance ($B_{M,imb}$). Turbine loads are also sensitive to twist distribution (ϕ), blade mass (B_M), and the C_1 distribution at the inboard section of the blade ($C_{1,b}$). Though these results are expected, their relative importance is likely a new finding. Other input parameters that were found to affect turbine load sensitivity are inboard maximum AoA ($\alpha_{max,b}$), blade mass center of mass (B_{CM}), blade flapwise stiffness (B_{FK}), nacelle center of mass location (N_{CM}), nacelle mass (N_{mass}), chord length at the inboard section of the blade (c_b), tower stiffness (T_{KF}), drivetrain damping (D_D), and inboard trailing edge separation AoA ($\alpha_{TES,b}$). The AoA values at the inboard section of the blade are likely more important than at the outboard section due to the higher likelihood of the inboard section operating with higher AoA near stall. Additionally, the range of AoA values at the inboard section is larger than at the outboard section because the nominal inboard AoA values are higher, which could contribute to greater sensitivity.
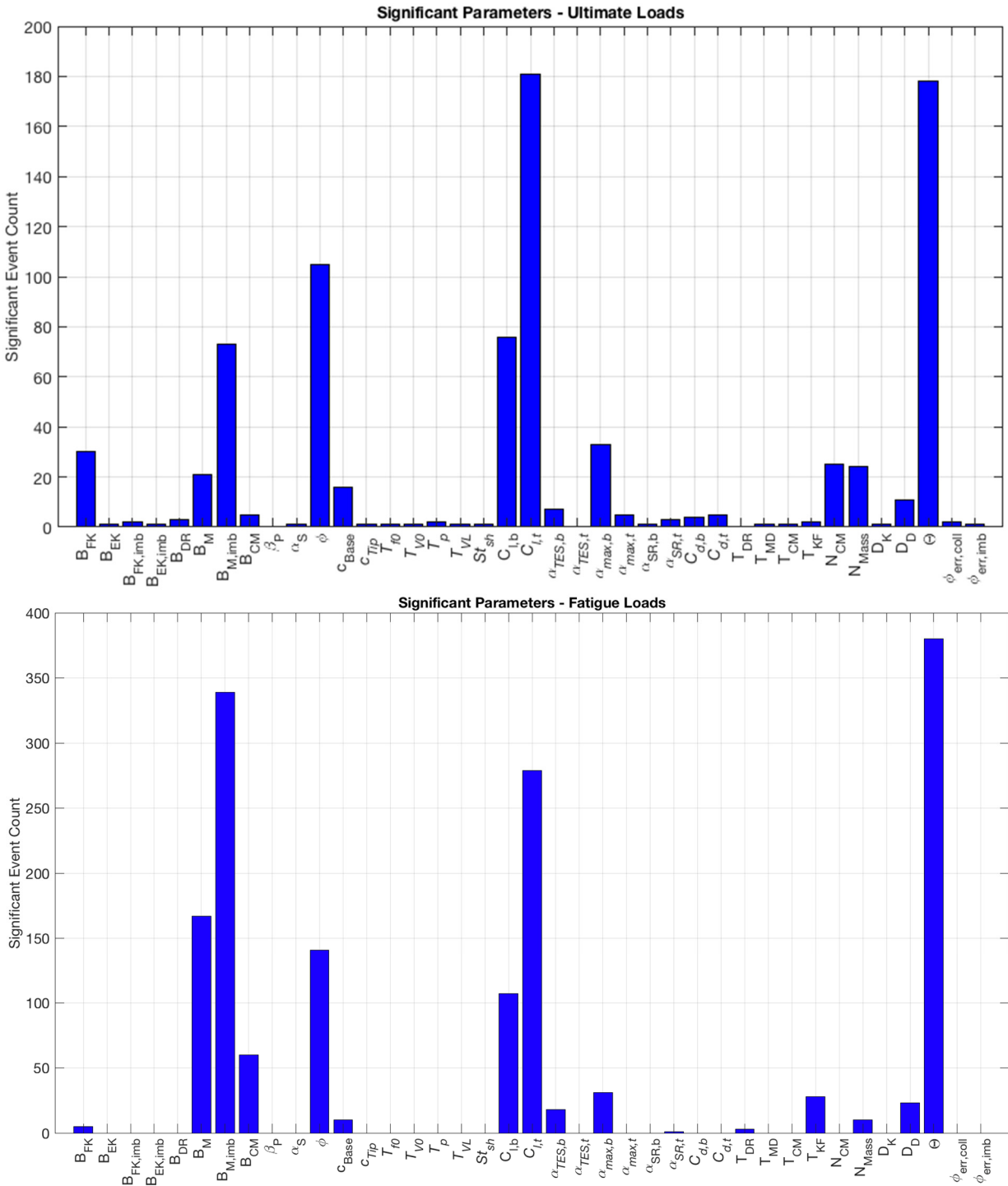
Figure 11: Identification of significant parameters using ultimate (top) and fatigue loads (bottom). Significant events are defined by the number of outliers identified across each of the QoIs for all wind speed bins, input parameters, and simulation points.

Table 11. Percentage of contribution to total number of significant events for ultimate and fatigue loads.

	θ (deg)	$B_{M,imb}$ (-)	$C_{l,t}$ (-)	$\emptyset$ (deg)	B_M (-)	$C_{l,b}$ (-)	$\alpha_{max,b}$ (deg)	B_{CM} (-)	B_{FK} (-)	N_{CM} (m)	N_{mass} (kg)	$\alpha_{TES,b}$ (deg)	c_b (m)	T_{KF} (m)	D_D (m)
Ult. Load (%)	21.5	8.8	21.9	12.7	2.5	9.2	4.0	0.6	3.6	3.0	2.9	0.8	1.9	0.2	1.3
Fat. Load (%)	23.7	21.2	17.4	8.8	10.4	6.7	1.9	3.7	0.3	0.0	0.6	1.9	0.6	1.7	1.4

Histograms of the EE values for each of the QoIs are plotted in Figure 12 - Figure 15 for the ultimate and fatigue load metrics (associated exceedance probability plots are shown in Appendix B; Figure 23 and Figure 24). Here, EE values are colored by
5 wind speed and the black vertical line represents the threshold for each QoI. The sharp separation of ultimate load EE values between wind speed bins is evident in Figure 12. A zoomed-in view of the lower count values is shown in Figure 13. The more evenly distributed nature of the fatigue load EE values is further highlighted in the histogram plots depicted in Figure 14 and zoomed in Figure 15. Unlike ultimate load EE values, all wind speed bins contribute to the outlier count for each QoI. Histogram plots of blade-root ultimate and fatigue bending moment EE values are shown in Figure 16 and Figure 17,
10 respectively. The sharp separation of ultimate load EE values between wind speed bins is again evident. Highlighted in the fatigue load plots is the more even distribution of threshold-exceeding EE values across wind speed bins.

The grouping of the results by wind speed bin creates an unequal distribution of outliers resulting from each turbine QoI. Most notably, blade-root pitching moment accounts for 18% of the total ultimate load significant events, whereas rotor torque accounts for only 5%. This suggests that it may be better to tailor the threshold for each QoI, but this was deemed overly
15 complicated for this first pass at assessing the sensitivity. Additionally, for a given QoI, it is typical for all ultimate load significant events to occur from either the near- or above-rated wind speeds. However, fatigue load EE values are more evenly distributed across wind speed bins, as shown in Figure 14. The lower significant event counts for ultimate loads is a result of the segregated nature of the ultimate load EE values, as opposed to the more evenly distributed nature of the fatigue load EE values. In fact, unlike ultimate load EE values, a large percentage of significant events result from below-rated wind speed
20 cases because of the higher probability of low wind speed conditions. However, the distribution of fatigue load outliers resulting from each turbine QoI is approximately the same as the distribution for ultimate load outliers, with 14.6% of outliers resulting from the blade-root OoP bending moment and only 4.3% resulting from the blade-root pitching moment. Note that the QoI (blade-root pitching moment) that contributed the most outliers for ultimate load outliers contributes the least for fatigue load outliers.
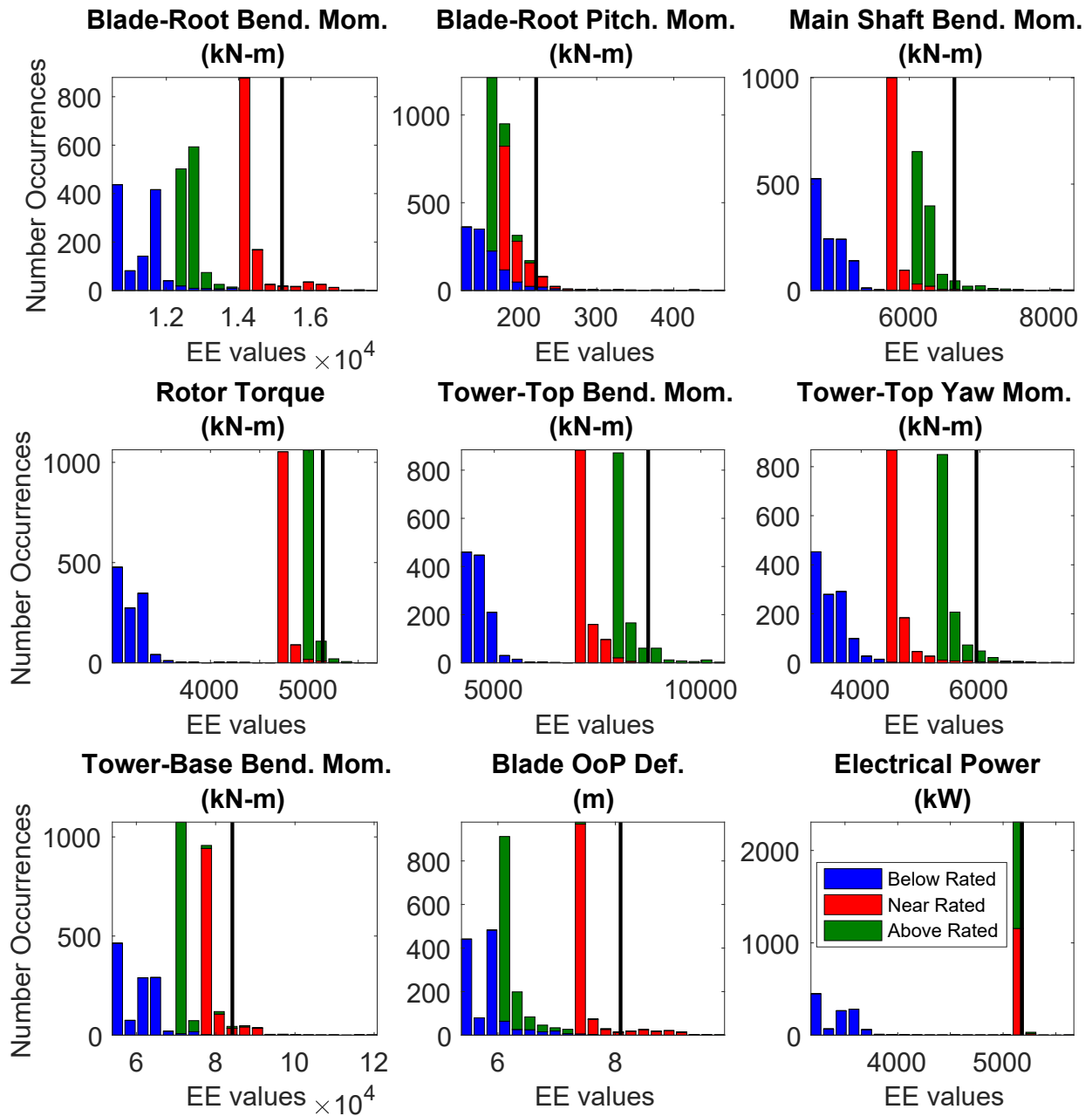
Figure 12: Stacked EE-values histograms of ultimate loads across all wind speed bins, input parameters, and simulation points for all QoIs. The black line represents the threshold by which outliers are counted for each QoI. Color indicates wind speed bin (blue=below rated, red=near rated, green=above rated).
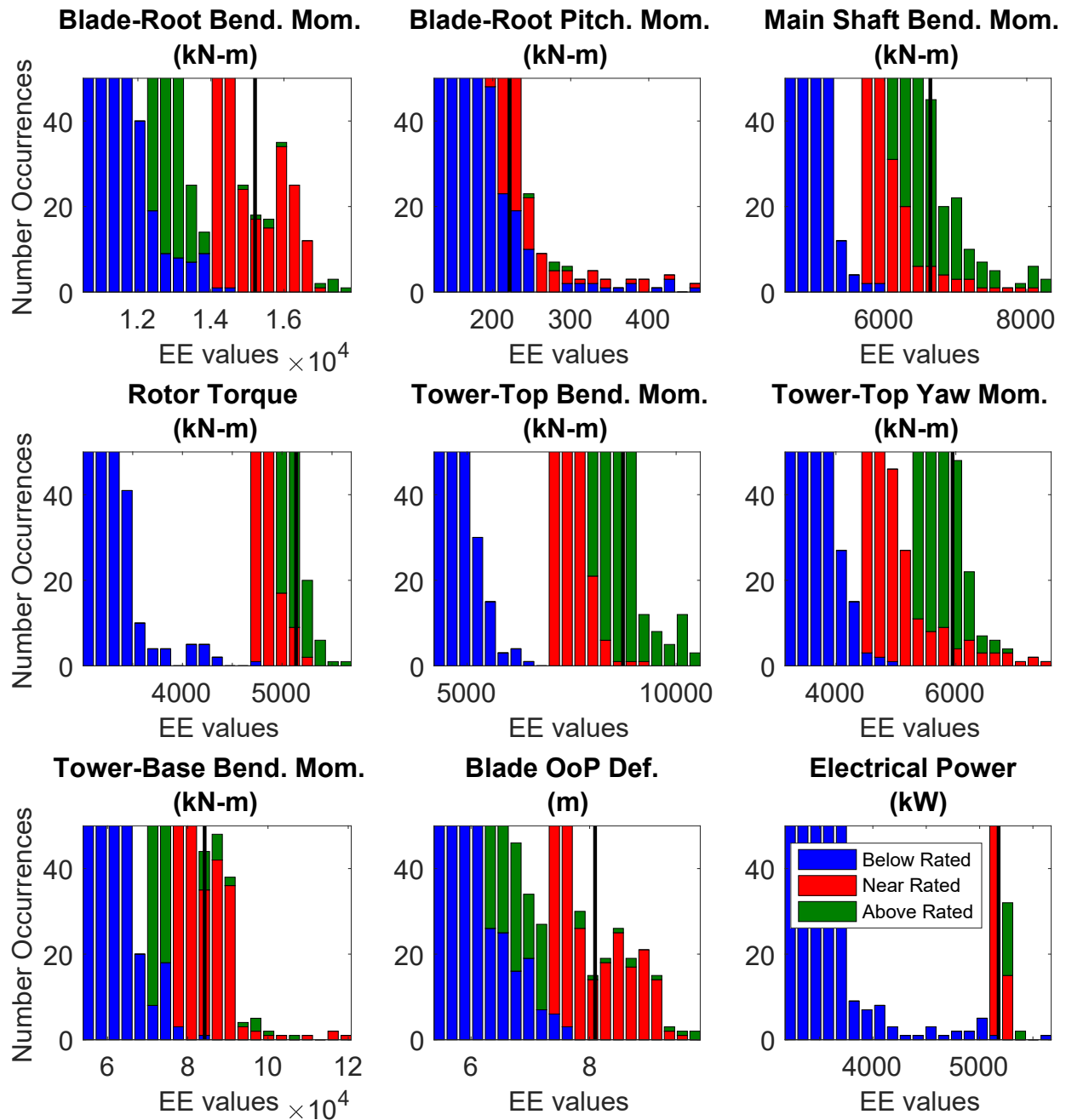
Figure 13: Zoomed-in stacked EE-values histograms of ultimate loads across all wind speed bins, input parameters, and simulation points for all QoIs. The black line represents the threshold by which outliers are counted for each QoI. Color indicates wind speed bin (blue=below rated, red=near rated, green=above rated).
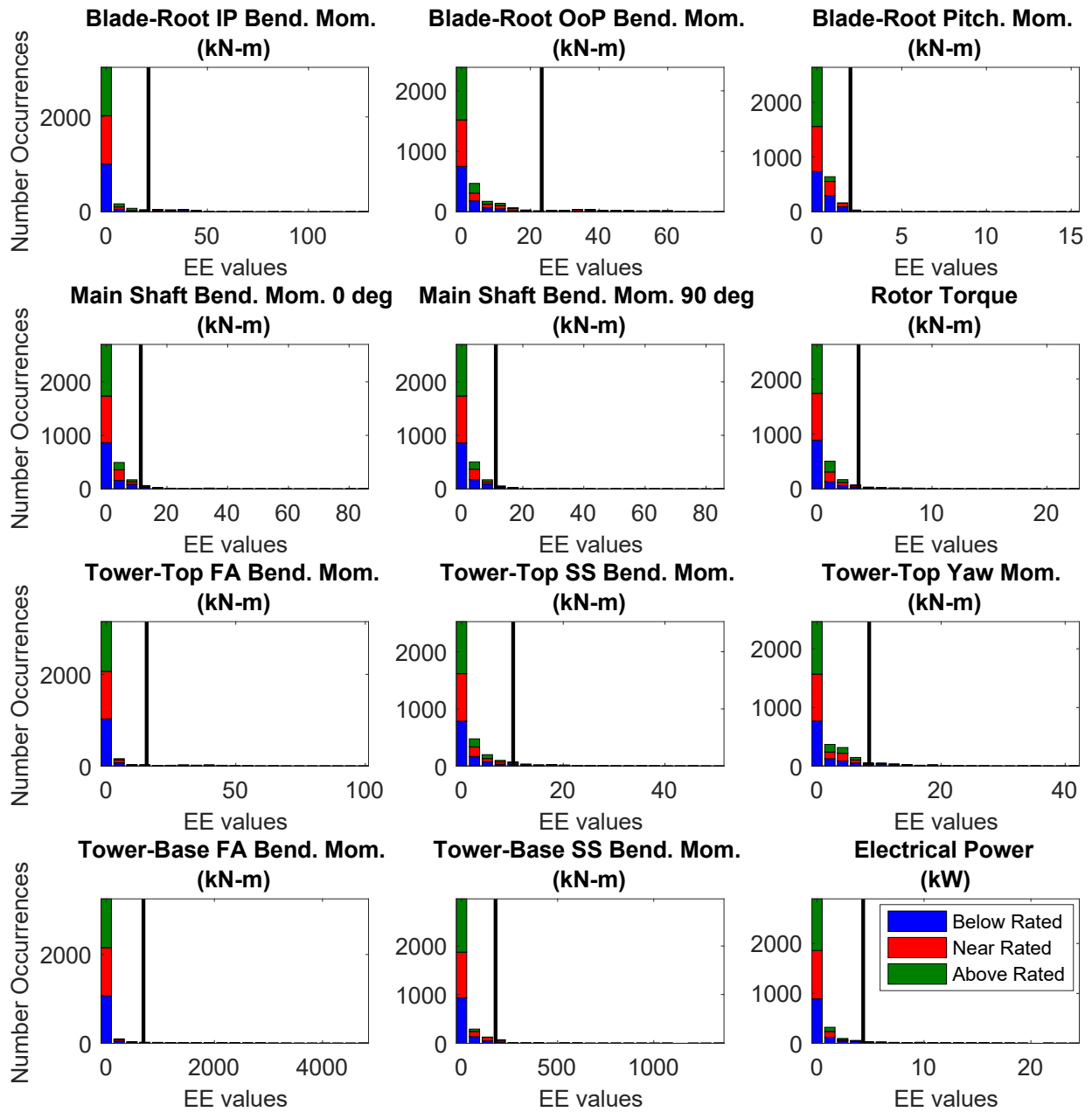
Figure 14: Stacked EE-values histograms of fatigue loads across all wind speed bins, input parameters, and simulation points for all QoIs. The black line represents the threshold by which outliers are counted for each QoI. Color indicates wind speed bin (blue=below rated, red=near rated, green=above rated).
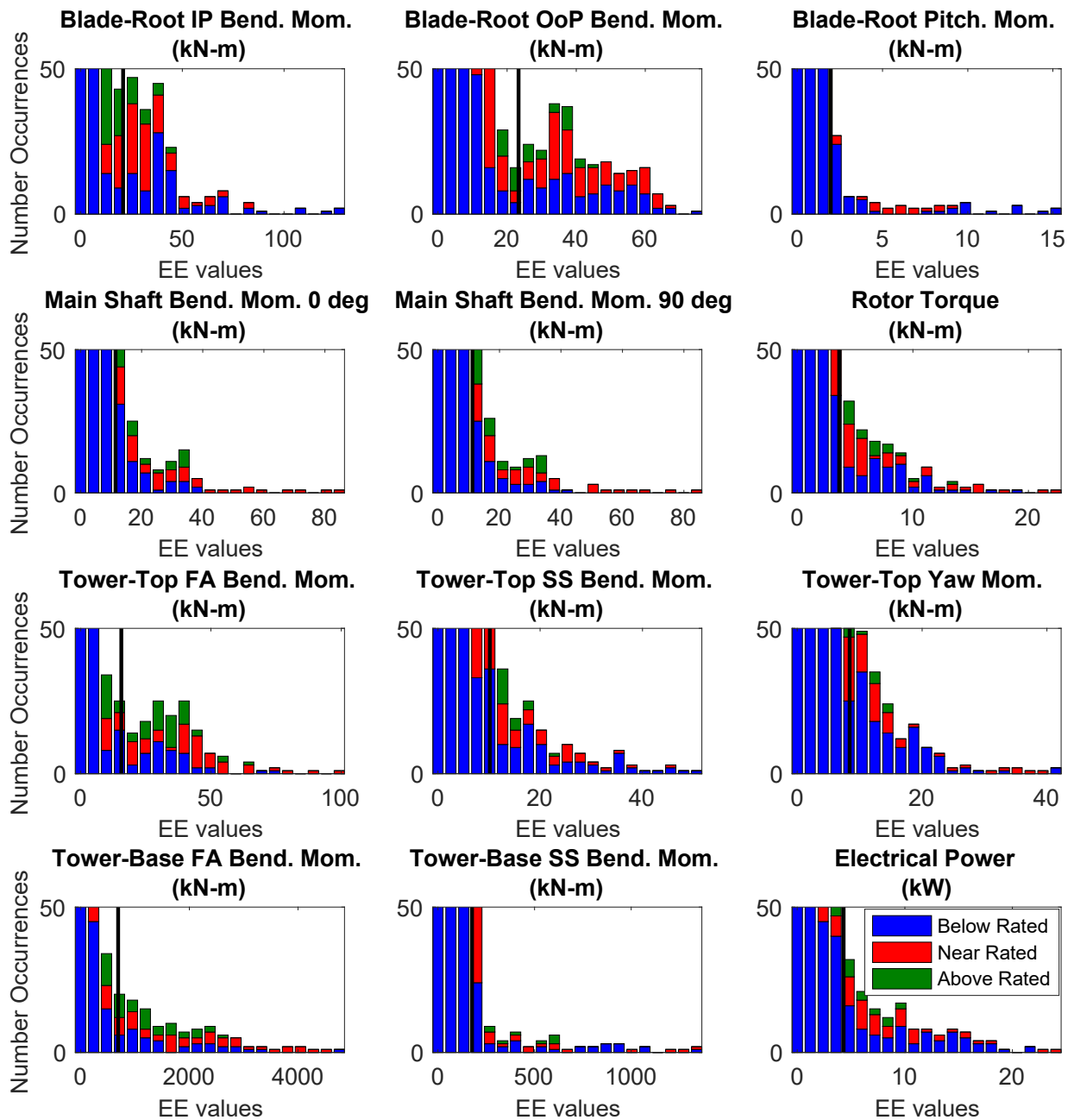
Figure 15: Zoomed-in stacked EE-values histograms of fatigue loads across all wind speed bins, input parameters, and simulation points for all QoIs. The black line represents the threshold by which outliers are counted for each QoI. Color indicates wind speed bin (blue=below rated, red=near rated, green=above rated).
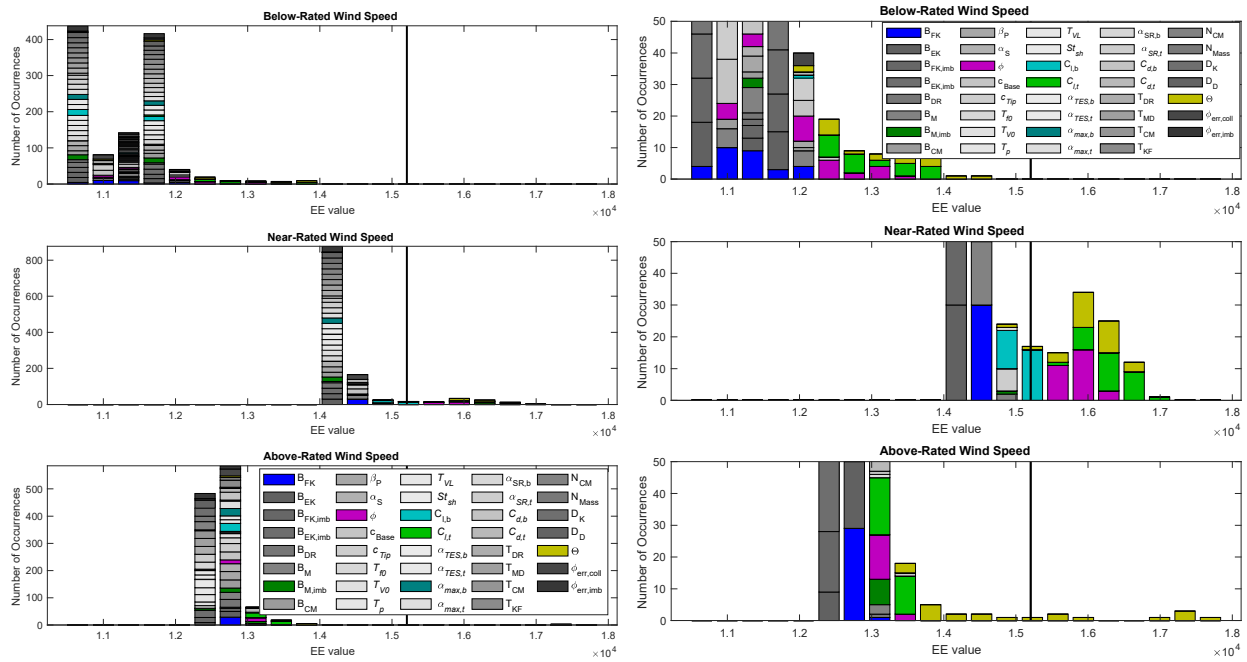
Figure 16: EE-values histograms of blade-root bending ultimate moment. Each graph shows one wind speed bin and includes all input parameters. Right column is a zoomed-in view of the left column.
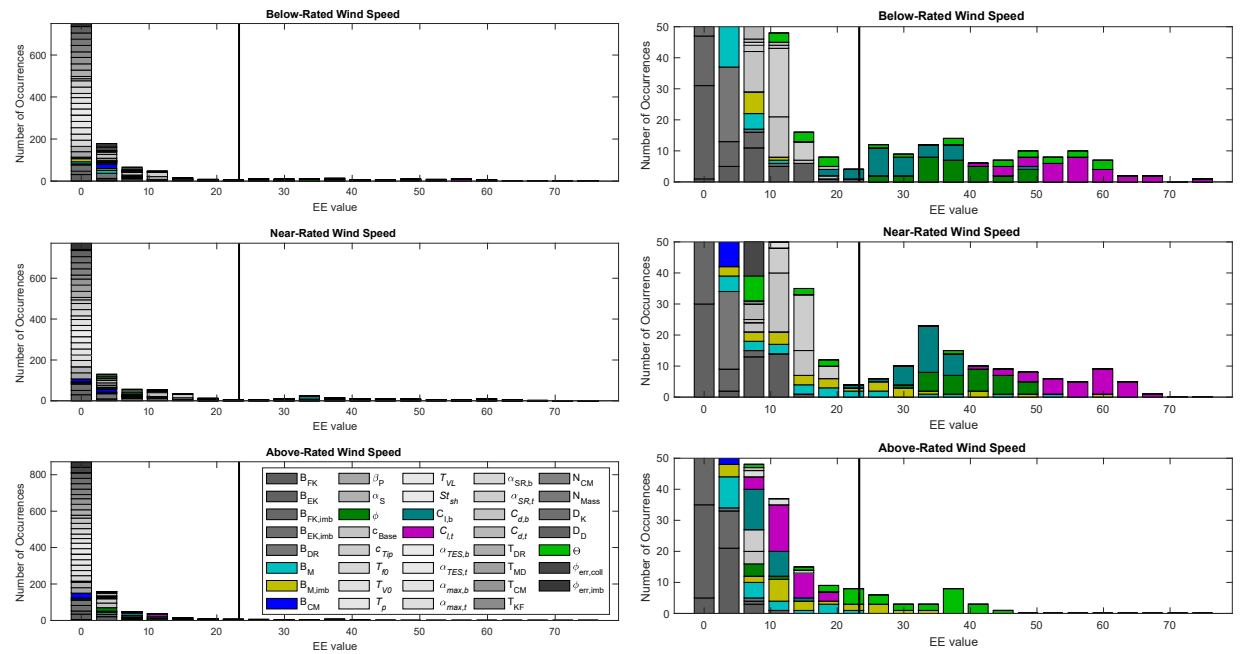
Figure 17: EE-value histograms of blade-root OoP bending fatigue moment. Each graph shows one wind speed bin and includes all input parameters. Right column is a zoomed-in view of the left column.

The behavior of blade-root loads are examined in more detail by plotting exceedance probability distinctly for each input parameter in Figure 18. Highlighted in these plots is the contribution of the individual input parameters to the outlier counts. For blade-root bending ultimate moment EE values, blade twist and $C_{l,t}$ EE values in the near-rated wind speed bin are beyond the threshold for every point in the hyperspace. Yaw error and $C_{l,b}$ EE values from the near-rated wind speed bin and yaw error from the above-rated wind speed bin also cross the threshold. For blade-root OoP bending fatigue moment EE values, the threshold is exceeded by blade twist and $C_{l,t}$ EE values from the below- and above-rated wind speeds for every point in the hyperspace. However, for all other relevant input parameters, only certain points in the hyperspace result in threshold exceedance. This indicates that, for certain loads and input parameters, the sensitivity of the turbine is dependent on the combination of turbine parameter values. These results can be used in future studies to more thoroughly investigate the hyperspace to determine how input parameter value combinations contribute to turbine sensitivity.
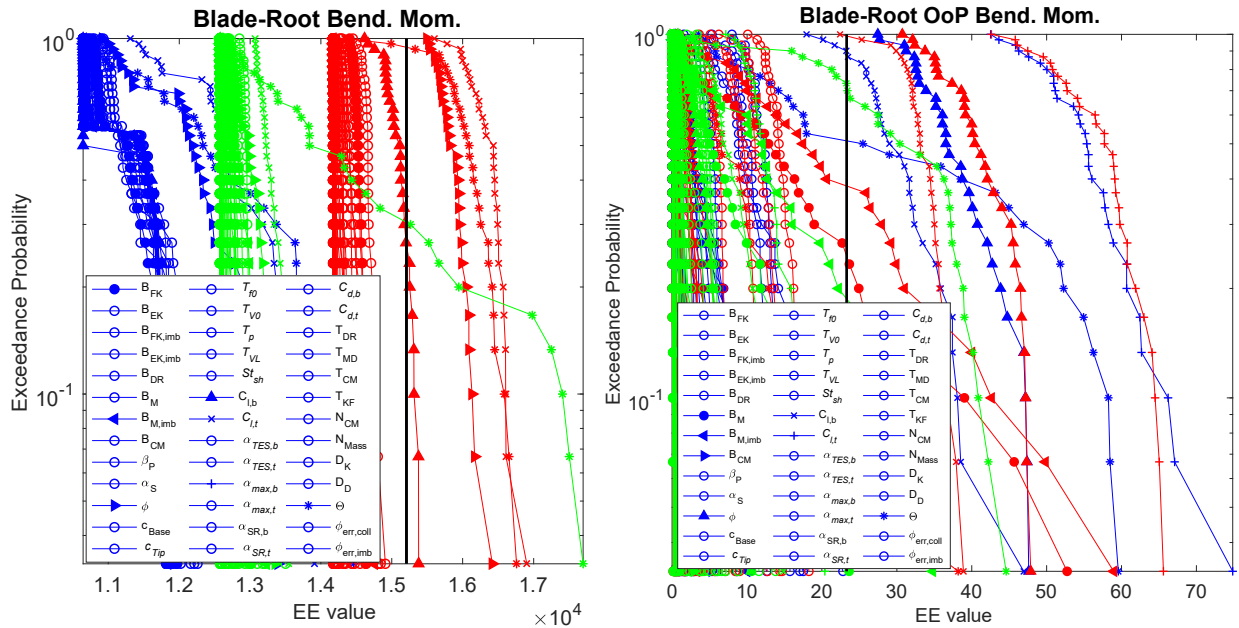
Figure 18: EE-value exceedance probability plots for the blade-root bending ultimate moment (left) and blade-root OoP bending fatigue moment (right). Each line represents a different input parameter and wind speed bin (blue=below rated, red=near rated, green=above rated).

For each QoI, the number of times each input parameter contributed to the significant event count was tallied. The top parameters are shown in Table 12 and Table 13 for ultimate and fatigue loads, respectively. Overall, 63% of the top sensitive parameters for both ultimate and fatigue loads are due to aerodynamic perturbations or yaw error. Blade-root and main shaft moments are especially sensitive to perturbations of inputs. However, blade mass imbalance and blade mass account for 44% of the most sensitive parameters associated with tower moment fatigue loads. Rotor torque ultimate and fatigue loads are most sensitive to perturbation of structural input parameters, especially those related to blade mass. For both ultimate and fatigue loads, electrical power is most sensitive to blade mass imbalance, blade mass factor, and yaw error. These results can be used in future sensitivity analysis work to focus on perturbation of specific input parameters based on desired turbine loads.

Table 12. Top input parameters contributing to ultimate load sensitivity of each QoI. Values indicate how many times the variable contributes to the sensitivity count.

Blade-Root Bend. Mom.	Blade-Root Pitch. Mom.	Main Shaft Bend. Mom.	Rotor Torque	Tower-Top Bend. Mom.	Tower-Top Yaw Mom.	Tower-Base Bend. Mom.	Blade OoP Deflection
θ (39)	$\alpha_{max,b}$ (33)	θ (43)	$B_{M,imb}$ (26)	θ (28)	$C_{l,t}$ (28)	$\phi/C_{l,t}$ (30)	$\phi/C_{l,b}$ (30)

$\phi/\,C_{l,t}$ (30)	$C_{l,b}$ (15)	$C_{l,t}$ (37)	D_D (25)	N_M (19)	θ (25)	$C_{l,b}$ (28)	B_{FK} (28)
$C_{l,b}$ (7)	ϕ (14)	c_b (22)	B_M (17)	$N_{CM}/C_{l,t}$ (17)	$C_{l,b}$ (21)	$B_{M,imb}$ (27)	θ (27)

Table 13. Top input parameters contributing to fatigue load sensitivity of each QoI. Values indicate how many times the variable contributes to the sensitivity count.

Blade-Root IP Bend. Moment	Blade-Root OP Pitch. Moment	Blade-Root Pitch. Moment	Main Shaft Bending Moment 0°	Main Shaft Bending Mom. 90°	Rotor Torque	Tower-Top FA Bend. Moment	Tower-Top SS Bend. Moment	Tower-Top Yaw Moment	Tower-Base FA Bend. Moment	Tower-Base SS Bend. Moment
B_{CM} (59)	$\phi/C_{l,t}$ (60)	$\alpha_{max,b}$ (31)	θ (49)	θ (49)	$B_{M,imb}$ (51)	θ (75)	θ (64)	$C_{l,t}$ (59)	$B_{M,imb}$ (59)	T_{KF} (28)
$B_{M,imb}$ (52)	$C_{l,b}$ (54)	$\alpha_{TES,b}$ (18)	$C_{l,t}$ (44)	$C_{l,t}$ (42)	θ (31)	$B_{M,imb}$ (54)	$C_{l,t}$ (52)	$B_{M,imb}$ (42)	B_M (48)	$B_{M,imb}$ (26)
B_M (47)	θ (36)	c_b (11)	ϕ (16)	ϕ (19)	B_M (28)	B_M (21)	$B_{M,imb}$ (38)	θ/ϕ (27)	T_{DR} (2)	$B_M/C_{l,t}/N_M$ (10)

Conclusions

A screening analysis of the most sensitive turbulent wind and aeroelastic parameters to the resulting structural loads and power QoI was performed for the representative NREL 5-MW wind turbine under normal operating conditions. The purpose of the study was to assess the sensitivity of different turbulent wind and turbine parameters on the resulting loads of the wind turbine. The sensitivities of the different parameters were ranked. The study did not consider specific site conditions, but rather focused on understanding the most sensitive parameters across the range of possible values for a variety of sites.

To limit the number of simulations required, a screening analysis using the EE method was used instead of a more computationally intensive sensitivity analysis. The EE method is an assessment of the local sensitivity of a parameter at a given location in space through variation of only that parameter, examined over multiple points throughout the parameter hyperspace, making it a global sensitivity analysis. This work modified the general EE formula to examine the sensitivity of parameters across multiple wind speed bins. A radial version of the method was employed, using Sobol numbers as starting points, and a set delta value of 10% for the parameter variations.

Two independent case studies were performed. For the wind parameter case study, it was found that the loads and power are highly sensitive to the shear and turbulence levels in the u-direction. To a lesser extent, turbine loads are sensitive to the wind veer and the integral length scale and coherence parameters in the u-direction. The combinations of parameters in this study spanned the ranges of several different locations. The parameters were considered independent of one another (conditioned only on wind speed bin), which likely resulted in some non-physical wind scenarios. However, the screening analysis has shown which parameters are most important to examine in more detail in future work.

The aeroelastic parameter case study showed that the loads and power are highly sensitive to the yaw error and the lift distribution at the outboard section of the blade. To a lesser extent, turbine loads are sensitive to blade twist distribution, lift distribution at the inboard section of the blade, and blade mass factor imbalance. Additionally, ultimate load EE values are typically separated by wind speed bin, whereas fatigue load EE values are more evenly distributed across wind speed bins.

Through the implemented EE method, different combinations of input parameters have been used. When specific input parameters are shown to be sensitive to one or more turbine loads, it is possible that only certain combinations of the input parameters will result in this sensitivity. This leads to opportunities for future work to further investigate which parameter combinations lead to higher turbine sensitivity. In future work, this ranking of most-sensitive parameters could be used to help establish error bars around predictions of engineering models during validation efforts and provide insight into probabilistic design methods and site-suitability analysis. While the most-sensitive ranking results may depend on the turbine size or

configuration, the analysis process developed here could be applied universally to other turbines. This work could also be further expanded in future work to include load cases other than normal operation.

Appendix A – Mean and Standard Deviation of Elementary Effects

To identify which parameters are the most sensitive, some researchers compare the average of the EE values for the different parameters across all input starting points. Additionally, some look at the standard deviation of the EE values for a given parameter across the different starting points. This helps to identify large sensitivity variation at different points, indicating strong interaction with the values of other parameters. As commonly found in EE-related literature, EE analysis typically identifies the most sensitive parameters using a plot to pictorially show the standard deviation versus mean values of the EE values. However, it is difficult to systematically identify the most sensitive parameters using this approach.

The mean of the absolute EE value for the ultimate loads for each QoI with input parameter i and bin b is calculated as:

$$\mu_{ib}^* = \frac{1}{R}\sum_{r=1}^{R}|EE_{ib}^r| \tag{11}$$

where R is the number of points at which the EE value is calculated. The standard deviation of the EE is then calculated as:

$$\sigma_{ib} = \sqrt{\frac{1}{(R-1)}\sum_{r=1}^{R}\left(EE_{ib}^r - \mu_{ib}\right)^2} \tag{12}$$

and μ_{ib} is defined as:

$$\mu_{ib} = \frac{1}{R}\sum_{r=1}^{R}EE_{ib}^r \tag{13}$$

This is shown in Figure 19 and Figure 20 for the blade-root bending ultimate moment and the blade-root bending OoP fatigue moment metrics for both the wind parameter and turbine parameter case studies, respectively. Shown in Figure 19 is the large sensitivity of shear in the lowest wind speed bin and the large sensitivity of the u-turbulence across all wind speed bins. Shown in Figure 20 is the large sensitivity of yaw error in the below-rated wind speed bin and the large sensitivity of the lift distribution at the outboard section of the blade in the below- and near-rated wind speed bins.
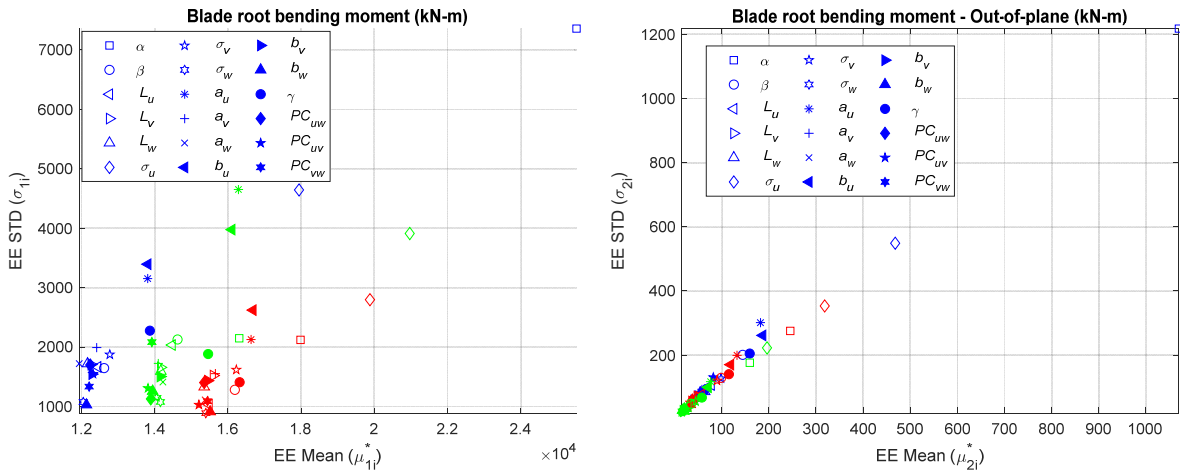
Figure 19: EE standard deviation vs EE mean for blade-root bending moment ultimate load (left) and blade-root out-of-plane bending moment fatigue load (right) at all wind speed bins (blue=below rated, red=near rated, green=above rated).
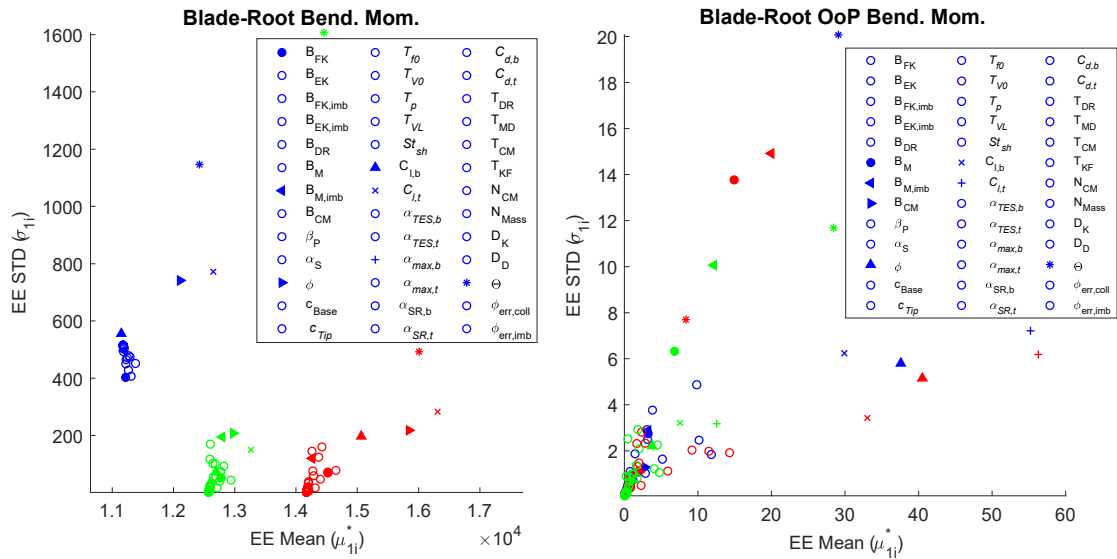
Figure 20: EE standard deviation vs EE mean for blade-root bending moment ultimate load (left) and blade-root out-of-plane bending moment fatigue load (right) at all wind speed bins (blue=below rated, red=near rated, green=above rated).

Appendix B – Exceedance Probability Plots of Elementary Effects
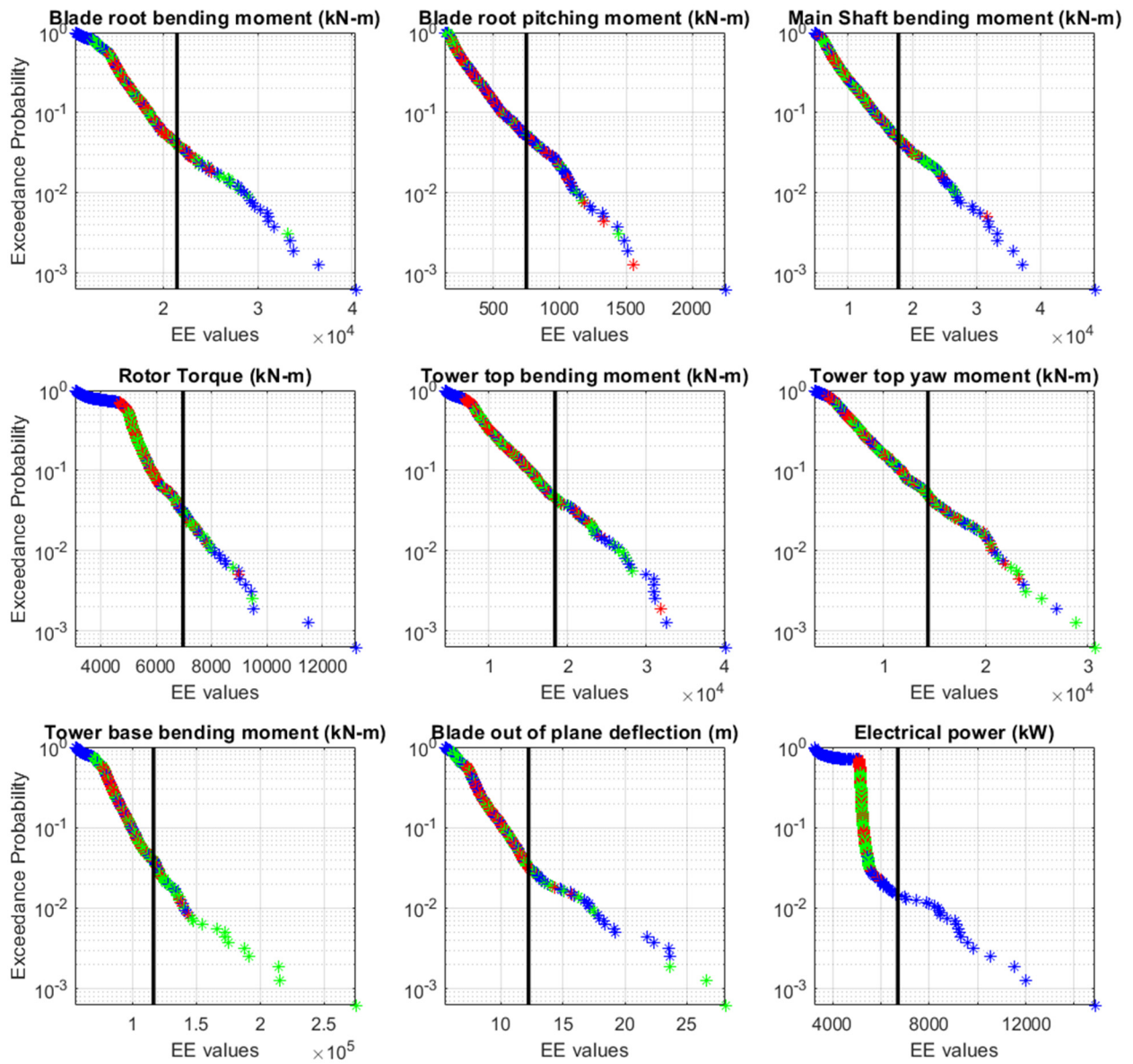
Figure 21: Exceedance probability plot of ultimate load EE values for each of the wind-inflow parameter QoIs across all wind speed bins, input parameters, and simulation points. Black line represents the defined threshold by which outliers are counted for each QoI. Color indicates wind speed bin (blue=below rated, red=near rated, green=above rated).
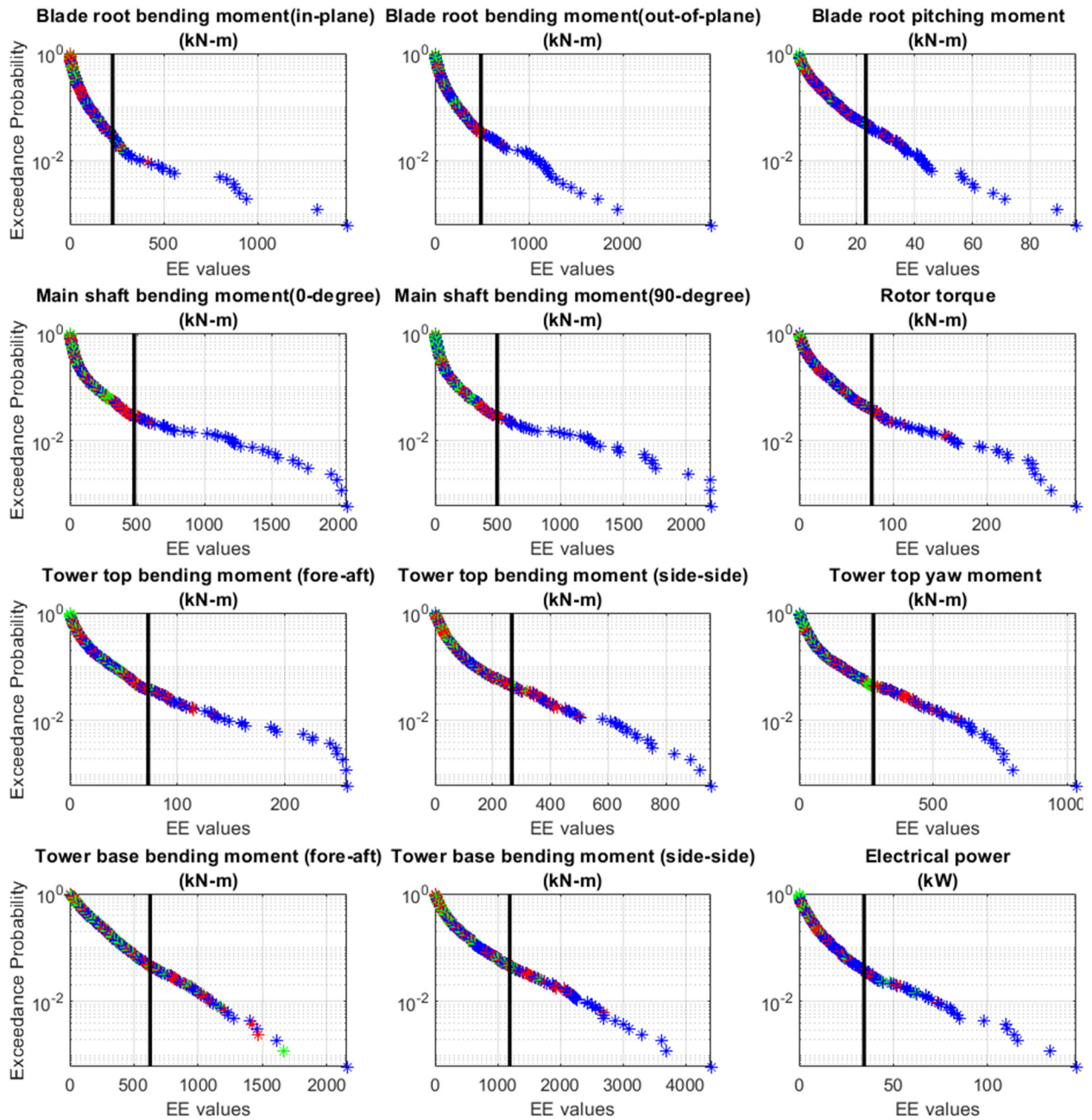
Figure 22: Exceedance probability plot of fatigue load EE values for each of the wind-inflow parameters across all wind speed bins, input parameters, and simulation points. Black line represents the defined threshold by which outliers are counted for each QoI. Color indicates wind speed bin (blue=below rated, red=near rated, green=above rated).
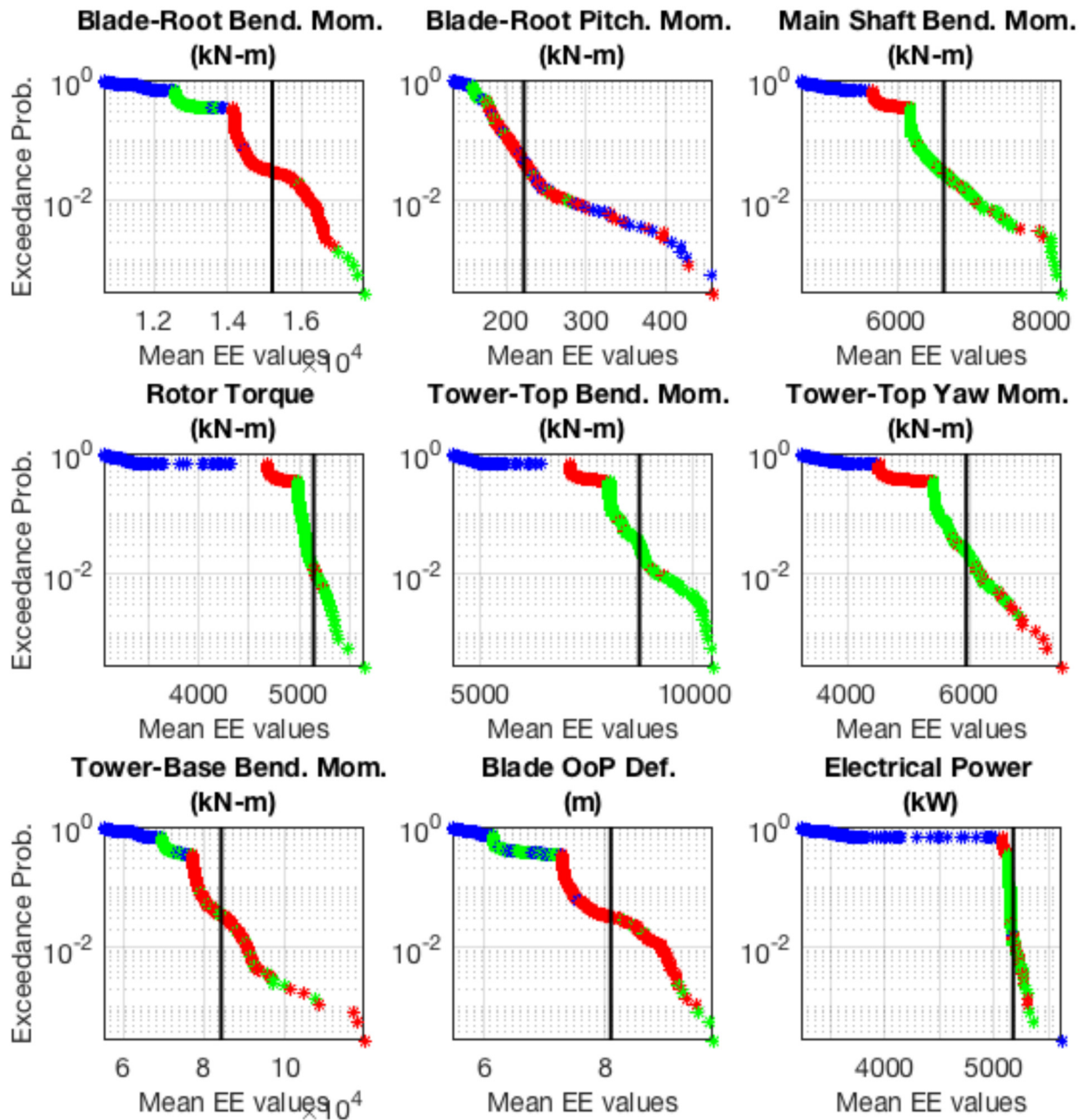
Figure 23: EE-value exceedance probability plots of ultimate loads for aeroelastic turbine parameters, across all wind speed bins, input parameters, and simulations points for all QoIs. The black line represents the defined threshold by which outliers are counted for each QoI. Color indicates wind speed bin (blue=below rated, red=near rated, green=above rated).
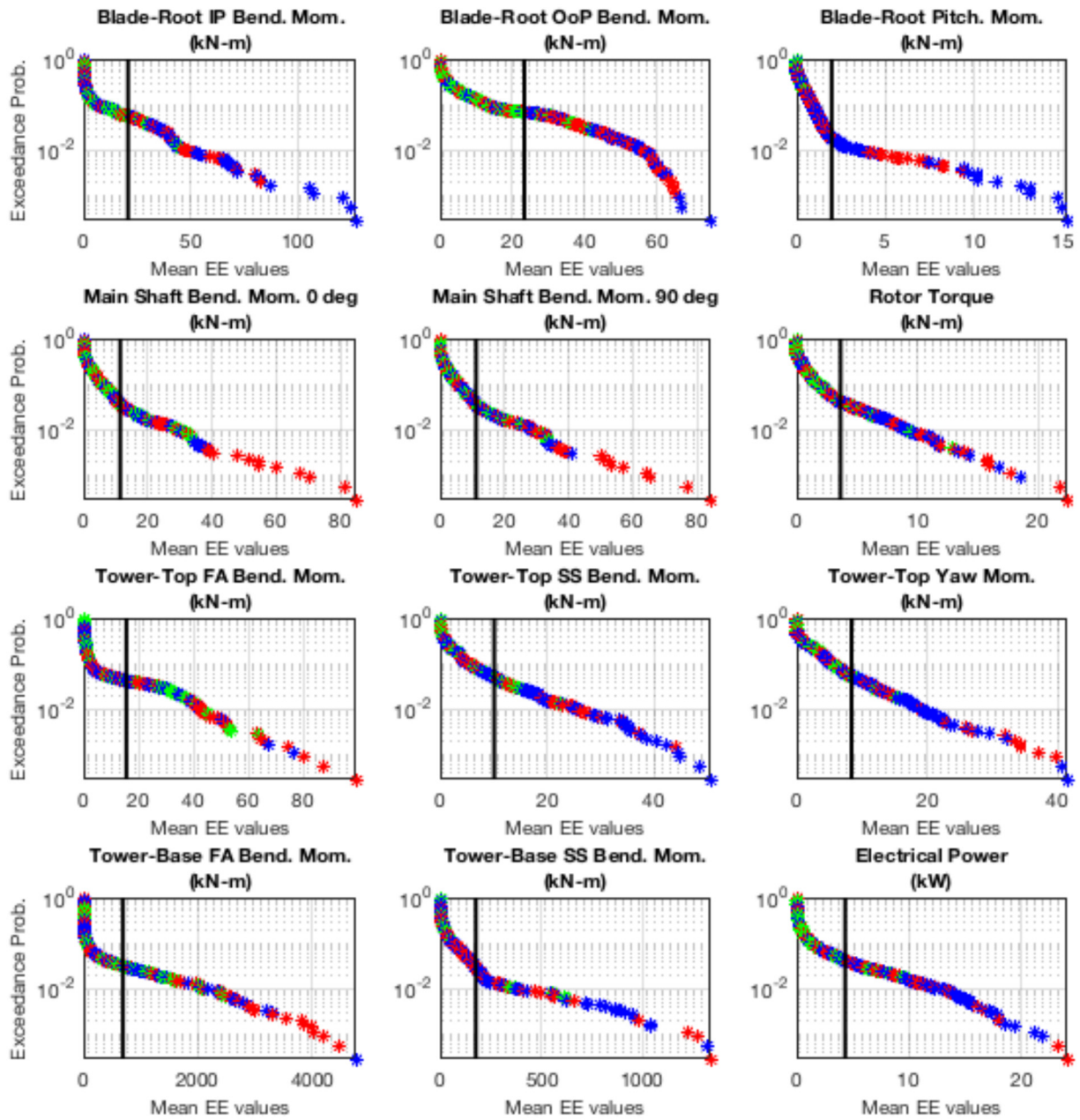
Figure 24: EE-value exceedance probability plots of fatigue loads of aeroelastic turbine parameters across all wind speed bins, input parameters, and simulations points for all QoIs. The black line represents the defined threshold by which outliers are counted for each QoI. Color indicates wind speed bin (blue=below rated, red=near rated, green=above rated).

Acknowledgements

This work was authored by Alliance for Sustainable Energy, LLC, the manager and operator of the National Renewable Energy Laboratory for the U.S. Department of Energy (DOE) under Contract No. DE-AC36-08GO28308. Funding provided by Department of Energy Office of Energy Efficiency and Renewable Energy, Wind Energy Technologies Office. The views expressed in the article do not necessarily represent the views of the DOE or the U.S. Government. The U.S. Government retains and the publisher, by accepting the article for publication, acknowledges that the U.S. Government retains a nonexclusive, paid-up, irrevocable, worldwide license to publish or reproduce the published form of this work, or allow others to do so, for U.S. Government purposes.

References

1. Abdallah, G., Natarajan, A., and Sorensen, J., "Impact of Uncertainty in Airfoil Characteristics on Wind Turbine Extreme Loads," *Renewable Energy*, Vol. 75, 2015, pp. 283–300. doi:10.1016/j.renene.2014.10.009.

2. Abdallah, I., Natarjan, A., and Sorenson, J.. "Assessment of extreme design loads for modern wind turbines using the probabilistic approach," DTU Wind Energy (DTU Wind Energy PhD; No. 0048(EN)), 2015.

3. Berg, J., Mann, J., and Patten, E.G., "Lidar-Observed Stress Vectors and Veer in the Atmospheric Boundary Layer," *Journal of Atmospheric and Oceanic Technology*, Vol. 30, September 2013.

4. Bulaevskaya, V., Wharton, S., Cliftons, A., Qualley, G., and Miller, W., "Wind Power Curve Modeling in Complex Terrain Using Statistical Models," *Journal of Renewable and Sustainable Energy*, vol. 7, 2015.

5. Burton, T., Jenkins, N., Sharpe, D., and Bossanyi, E., *Wind Energy Handbook*, 2011.

6. Campolongo, F., Cariboni, J., and Saltelli, A., "An Effective Screening Design for Sensitivity Analysis of Large Models," *Environmental Modelling and Software* Vol. 22, 2007, pp. 1509–1518.

7. Campolongo, F., Saltelli, A., and Cariboni, J., "From Screening to Quantitative Sensitivity Analysis. A Unified Approach," *Computer Physics Computations*, Vol. 182, 2011, pp. 978–988.

8. Clifton, A., "135-m Meteorological Towers at the NWTC: Instrumentation, Data Acquisition and Processing," *Draft, https://wind.nrel.gov/MetData/Publications/.*

9. Crestaux, T., Maitre, O., and Martinez, J., "Polynomial Chaos Expansion for Sensitivity Analysis," *Reliability Engineering and System Safety*, Vol. 94, 2009, pp. 1161–1172.

10. Damiani, R. R., Hayman, G. J., and Jonkman, J., "Development and Validation of a New Unsteady Airfoil Aerodynamics Model Within AeroDyn," *AIAA SciTech Forum*, AIAA, San Diego, CA, 2016, pp. 1–21. doi:10.2514/6.2016-1007.

11. Damiani, R., personal communication, May 2018.

12. Dimitrov, N., and Berg, J., "2016 CCA: Wind2loads," *Presentation at Wind2loads Industry Webinar*, February 22nd, 2017.

13. Dimitrov, N., Natarajan, A., and Kelly, M., "Model of Wind Shear Conditional on Turbulence and Its Impact on Wind Turbine Loads," *Wind Energy*, Vol. 18, 2015, pp. 1917–1931.

14. Downey, R., "Uncertainty in Wind Turbine Life Equivalent Load due to Variation of Site Conditions," *M.Sc. Thesis Project* for the Technical University of Denmark, 2006.

15. Eggers, A., Digumarthi, R., and Chaney, K., "Wind Shear and Turbulence Effects on Rotor Fatigue and Loads Control," *Transactions of the ASME*, Vol. 125, November 2003.

16. Ehrmann, R.S., Wilcox, B., White, E. B., and et al., "Effect of Surface Roughness on Wind Turbine Performance," Tech. Rep. SAND2017-10669, Sandia National Laboratory, Albuquerque, NM, October 2017.

17. Ernst, B., and Seume, J., "Investigation of Site-Specific Wind Field Parameters and Their Effect on Loads of Offshore Wind Turbines," *Energies*, Vol. 5, 2012, pp. 3835–3855.

18. Francos, A., Elorza, F., Bouraoui, F., Bidoglio, G., and Galbiati, L., "Sensitivity Analysis of Distributed Environmental Simulation Models: Understanding the Model Behavior in Hydrological Studies at the Catchment Scale," *Reliability Engineering and System Safety*, Vol. 79, 2003, pp. 205–218.

19. Gan, Y. and et al., "A Comprehensive Evaluation of Various Sensitivity Analysis Methods: A Case Study with a Hydrological Model," *Environmental Modelling and Software*, Vol. 51, 2014, pp. 269–285.

20. Gan, Y. and et al., "A Comprehensive Evaluation of Various Sensitivity Analysis Methods: A Case Study with a Hydrological

21. Hayman, G. and Buhl, J. (2012). "MLife User's Guide for Version 1.00," NREL Technical Report, downloaded from: https://nwtc.nrel.gov/system/files/MLife_User.pdf.

22. Holierhoek, J.G., Korterink, H., van de Pieterman, R.P., Braam, H., Rademakers, L.W.M.M., and et al. (2010). "PROTEST: Recommended Practices for Measuring in Situ the 'Loads' on Drive Train, Pitch System, and Yaw System". ECN, PROTEST project deliverable D6, D7, D8.

23. Holtslag, M., Bierbooms, W., and Bussel, G., "Wind Turbine Fatigue Loads as a Function of Atmospheric Conditions," *Wind Energy,* Vol. 19, 2016, pp. 1917–1932.

24. Huang, Y. and Pierson, D., "Identifying Parameter Sensitivity in Water Quality Model of a Reservoir," *Water Quality Research Journal of Canada*, Vol. 47, 2012, pp. 451–462.

25. IEC, "IEC 61400–1 Ed. 3. Wind Turbines – Part 1: Design Requirements," 2005.

26. IEC, "IEC 61400–5 Ed. 3. Wind Turbines – Part 5: Rotor Blades Wind Turbines," 2010.

27. Jansen, M., "Analysis of Variance Designs for Model Output," *Computer Physics Communication*, Vol. 117, 1999, pp. 35–43.

28. Jonkman, B. "TurbSim User's Guide v1.50", NREL/TP-500-46198, 2009.

29. Jonkman, J., Butterfield, S., Musial, W., and Scott, G., "Definition of a 5-MW Reference Wind Turbine for Offshore System Development," NREL/TP-500-38060, Golden, CO: National Renewable Energy Laboratory, February 2009.

30. Kalverla, P., Steeeveld, G., Ronda, R., and Holtslag, A., "An Observational Climatology of Anomalous Wind Events at Offshore Meteomast Ijmuiden (North Sea)," *Journal of Wind Engineering and Industrial Aerodynamics*, Vol. 165, 2017, pp. 86–99.

31. Kelley, N., "Turbulence-Turbine Interaction: The Bases for the Development of the TurbSim Stochastic Simulator," NREL Report TP-5000-52353, 2011.

32. Kelly, M., Larsen, G., Dimitrov, N., and Natarjan, A., "Probabilistic Meteorological Characterization for Turbine Loads," *The Science of Making Torque from Wind*, Vol. 524, 2014.

33. Koukoura, C., "Validated Loads Prediction Models for Offshore Wind Turbines for Enhanced Component Reliability," DTU Wind Energy (DTU Wind Energy PhD; No. 0026 (EN), 2014.

34. Lindelöw-Marsden, P., "Uncertainties in Wind Assessment with LIDAR," *Risø-R-1681UpWind Deliverable D1*, Risø National Laboratory for Sustainable Energy, Technical University of Denmark, January 2009.

35. Loeven, G.J.A. and Bijl, H., "Airfoil Analysis with Uncertain Geometry Using the Probabilistic Collection Method," *AIAA Structures, Structural Dynamics, and Materials Conference*, 2008.

36. Madsen, H. A., Bak, C., Paulsen, U. S., and et. al, "The DAN-AERO MW Experiments Final Report," Tech. Rep. Risø-R-1726 (EN), Risø DTU, Roskilde, Denmark, September 2010.

37. Martin, R., Lazakis, I., Barbouci, S., and Johanning, L., "Sensitivity Analysis of Offshore Wind Farm Operation and Maintenance Cost and Availability," *Renewable Energy*, Vol. 85, 2016, pp. 1226–1236.

38. Matthuas, D., Bortolotti, P., Loganathan, J., and Bottasso, C., "A Study of the Propagation of Aero and Wind Uncertainties and their Effect on the Dynamic Loads of a Wind Turbine," *AIAA SciTech Forum*, 2017.

39. Moriarty, P., Holley, W., and Butterfield, S., "Effect of Turbulence Variation on Extreme Loads Prediction of Wind Turbines," *Journal of Solar Energy Engineering*, Vol. 124, 2002, pp. 387–395.

40. Moroz, E., "Time to Upgrade the Wind Turbine Suitability Process," *Presentation at AWEA WindPower 2017*.

41. Nelson, L.D., Manuel, L., Sutherland, H.J., and Veers, P.S., "Statistical Analysis of Wind Turbine Inflow and Structural Response Data from the LIST Program," *Journal of Solar Energy Engineering,* Vol. 125, pp. 541–550, 2003.

42. "OpenFAST Documentation," November 2017. URL http://openfast.readthedocs.io/en/master.

43. Park, J., Manuel, L., and Basu, S., "Toward Isolation of Salient Features in Stable Boundary Layer Wind Fields that Influence Loads on Wind Turbines," *Energies*, Vol. 8, 2015.

44. Petrone, G., de Nicola, C., Quagliarella, D., Witteveen, J., and Iaccarino G., "Wind Turbine Performance Analysis Under Uncertainty," *AIAA Aerospace Sciences Meeting*, 2011.

45. Quick, J., Annoni, J., King, R., Dykes, K., Fleming, P., and Ning, A., "Optimization Under Uncertainty for Wake Steering Strategies," *Wake Conference*, Vol. 854, 2017.

46. Rinker, J., "Calculating the Sensitivity of Wind Turbine Loads to Wind Inputs Using Response Surfaces," *The Science of Making Torque from Wind*, Vol. 753, 2016.

47. Robertson, A. Sethuraman, J.; Jonkman, J.; Quick, J. "Assessment of Wind Parameter Sensitivity on Ultimate and Fatigue Wind Turbine Loads," *Presented at the American Institute of Aeronautics and Astronautics SciTech Forum,* Orlando, Florida January 8–12, 2018.

48. Saint-Geours, N. and Lilburne, L., "Comparison of Three Spatial Sensitivity Analysis Techniques," *Accuracy 2010 Symposium*.

49. Saltelli, A. and et al., *Global Sensitivity Analysis, The Primer*, 2008.

50. Santos, R. and van Dam, J. "Mechanical Loads Test Report for the U.S. Department of Energy 1.5-Megawatt Wind Turbine," NREL/TP-5000-63679, 2015.

51. Saranyasontoorn, K., Manuel, L., and Veers, P.S., "A Comparison of Standard Coherence Models for Inflow Turbulence with Estimates from Field Measurements," *Journal of Solar Energy Engineering*, Vol. 126, November 2004.

52. Saranyasoontorn, K. and Manuel, L., "On the Study of Uncertainty in Inflow Turbulence Model Parameters in Wind Turbine Applications," *44ᵗʰ AIAA Aerospace Sciences Meeting and Exhibit*, 9–12 January 2006, Reno, Nevada.

53. Saraynsoontorn, K. and Manuel, L., "On the Propagation of Uncertainty in Inflow Turbulence to Wind Turbine Loads," *Journal of Wind Engineering and Industrial Aerodynamics,* Vol. 96, 2008, pp. 508–523.

54. Sathe, A., Mann, J., Barla, T., Bierbooms, A., and van Bussel, G., "Influence of atmospheric stability on wind turbine loads," *Wind Energy*, 2012.

55. Simani, S. and Castaldi, P., "Robust Control Examples Applied to a Wind Turbine Simulated Model," *Applied Sciences,* Vol. 8, 2017, pp. 1-28.

56. Simms, D., Schreck, S., Hand, M., and Fingersh, L., "NREL Unsteady Aerodynamics Experiment in the NASA-Ames Wind Tunnel: A Comparison of Predictions to Measurements," Tech. Rep. NREL/TP-500-29494, National Renewable Energy Laboratory, Golden, CO, June 2001.

57. Sohier, H., Piet-Lahanier, H., and Farges, J., "Analysis and Optimization of an Air-Launch-to-Orbit Separation," *Acta Astronautica*, Vol. 108, 2015, pp. 18–29.

58. Solari, G. and Piccardo, G., "Probabilistic 3-D Turbulence Modeling for Gust Buffeting of Structures," *Probabilistic Engineering Mechanics*, Vol. 16, 2001, pp. 73–86.

59. Solari, G., "Turbulence Modelling for Gust Loading," *ASCE Journal of Structural Engineering*, Vol. 113, no.7, 1987, pp. 1550–1569.

60. Sumner, T., Shephard, E., and Bogle, I., "A Methodology for Global-Sensitivity Analysis of Time-Dependent Outputs in Systems Biology Modelling," *Journal of the Royal Society Interface*, Vol. 9, 2012, pp. 2156–2166.

61. Sutherland, H., "Analysis of the Structural and Inflow Data from the LIST Turbine," Sandia National Laboratories Report, SAND2002-1838J, 2002.

62. Teunissen, H., "Characteristics of the Mean Wind and Turbulence in the Planetary Boundary Layer," *UTIAS 32*, Institute for Aerospace Studies, University of Toronto, 1970.

63. Wagner, R., Courtney, M., and Larsen, T., "Simulation of Shear and Turbulence Impact on Wind Turbine Performance," *Risø-R-Report 1722*, Jan. 2010.

64. Walter, K., Weiss, C., Swift, A., Chapman, J., and Kelley, N., "Speed and Direction Shear in the Stable Nocturnal Boundary Layer," *Journal of Solar Energy Engineering*, Vol. 131, 2009.

65. Wharton, S., Newman, J.F., Qualley, G., and Miller, W.O., "Measuring Turbine Inflow with Vertically-Profiling Lidar in Complex Terrain," *J. Wind Eng. Ind. Aerodyn.,* Vol. 142, 2015, pp. 217–231.

66. Witcher, D., "Uncertainty Quantification Techniques in Wind Turbine Design," *Presentation* 2017.

67. Ziegler, L. and Muskulus, M., "Fatigue Reassessment for Lifetime Extension of Offshore Wind Monopile Substructures," *The Science of Making Torque from Wind*, Vol. 753, 2016.